



Changes in mobility can relate to molecular states in large dense core vesicles

Dissertation
zur Erlangung des Grades
des Doktors der Naturwissenschaften
der Medizinischen Fakultät
der Universität des Saarlandes

vorgelegt von
Shahira Nofal Ibrahim El Sayed
M.Sc., Pharmacist

Homburg
2007

Tag der mündlichen Prüfung:

1. Gutachter: Prof. Dr. Jens Rettig
2. Gutachter: Prof. Dr. Joachim Deitmer

Acknowledgment

I would like to thank my supervisor Prof. Dr. Jens Rettig who supported me and my work with advice and discussions and who had enough confidence in me to have me work on this special project.

I am also very grateful for all the help that Dr. Ute Becherer gave me from beginning to end. She has taught me all I know about fluorescence and I hope that she will continue to advise me on my future ventures.

I would like to thank Dr. Detlef Hof for his extreme patience and for providing us with the tracking programs and analyzing methods that were used in this work and for realising all our wishes regarding computer programs.

I also thank Dr. Ulf Matti for providing me with all the viral compounds used in this project and for helping me in many other ways.

I am thankful for Dr. David Stevens' help and support. He helped with very stimulating and lively discussions and for critical reading of this manuscript.

I also thank Dr. Claudia Schirra, Dr. Kailai Duan and Mathias Pasche for their support in various situations and for making life easier.

I would also like to thank Reiko Trautmann, Manuela Schneider, Carolin Bick, Ulrike Klemstein and Katrin Sandmeier for their support. Without them, this project would have gone on endlessly. My deepest thanks go to all those who helped with the smallest advice.

Last but not least, I thank my husband Sameh for his support and extreme patience, my father, Nofal Ibrahim, for putting me on the highway to science; my mother, Nabiha Mahmoud, for absorbing all my stress even overseas and of course my angel, Shorouk, for making life look funny even when it wasn't.

I hereby certify that the present work was solely performed using the methods described therein. Any external information or data was cited in its respective place. This work has not been published anywhere in its present form and is the means to attain an academic grade.

Homburg, 9-10-2007

Shahira Nofal

List of contents

List of contents	I
Zusammenfassung	III
Abbreviations	V
1. Introduction	1
1.1. Secretion: an essential process	1
1.2. Chromaffin cells: A model of regulated exocytosis.	2
1.3. Molecular changes prior to membrane fusion in chromaffin cells	4
1.4. Proteins involved in exocytosis	7
1.5. Proteins involved in docking	11
1.6. Proteins involved in priming	12
1.7. Total internal reflection fluorescence microscopy (TIRFM)	14
1.8. Aim of the work	17
2. Materials and Methods	19
2.1 Materials	19
2.1.1 Reagents	19
2.1.2 Enzymes	21
2.1.3 Plasmids	21
2.1.4 Media and solutions	21
2.1.4.1 Solutions for chromaffin cell preparation	21
2.1.4.2 Solutions for BHK cell culture/virus generation and activation	22
2.1.4.3 Solutions for TIRFM experiments	24
2.1.4.4 Solutions for whole-cell patch experiments	24
2.2 Methods	25
2.2.1 Bovine chromaffin cell preparation	25
2.2.2 Protocol for electroporation	26
2.2.3 Protocol for virus generation, activation and infection	26
2.2.3.1 Cultivation of BHK21 cells	26
2.2.3.2 Preparation of viral RNA	27
2.2.3.2.1 Linearization of DNA	27
2.2.3.2.2 In-vitro transcription	28
2.2.3.2.3 Quantification of RNA amount by electrophoresis	28
2.2.3.3 Electroporation of BHK21 cells with RNA	29
2.2.3.3.1 Virus titer test	29
2.2.3.4 Infection of bovine chromaffin cells	30

2.2.4	TIRFM	30
2.2.4.1	Setup	30
2.2.4.2	Experimental protocols	31
2.2.5	Analysis of movies	32
2.2.6	Analysis of caging diameter	35
2.2.7	Statistical analysis	38
3.	Results	39
3.1	Effect of PMA on bovine chromaffin cells	39
3.1.1	Effect on secretion	39
3.1.2	Mobility of vesicles in cells treated with PMA	41
3.2	Determination of limits of mobility	44
3.2.1	PMA treatment increases the number of nearly immobile vesicles	47
3.3	Overexpression of Munc13-1 alone and fused with NPY-mRFP.	49
3.4	Effect of Munc13-1 on secretion from chromaffin cells	50
3.4.1	Munc13-1 increases secretory events observed in TIRFM	50
3.4.2	Munc13-1 overexpression increases the number of immobile vesicles	53
3.5	Overexpression of tetanus toxin light chain increases the mobility of vesicles	56
4.	Discussion	60
4.1	The caging diameter: a novel method to analyze motion	60
4.2	Secreted vesicles motion is different	62
4.3	Priming leads to a reduction in the LDCV mobility	63
4.4	Mobility of LDCVs increases when priming is prevented	66
4.5	Perspectives	67
5.	Summary	69
6.	Literature	71
	Curriculum Vitae	79
	Publications	80

Zusammenfassung

Die Fusion von Vesikeln mit der präsynaptischen Membran ist der letzte Schritt bei der Ausschüttung von Neurotransmittern und vielen weiteren Signalmolekülen. Vor dem eigentlichen Fusionsereignis durchlaufen die synaptischen Vesikel mehrere Reifungsprozesse, wobei die freien Vesikel erst an der Membran verankert (Docking) und dann für die Fusion vorbereitet werden (Priming).

Exozytose lässt sich mit Hilfe von elektrophysiologischen Messungen sehr gut untersuchen, dabei ist der Fusionsschritt direkt messbar, während für das Docking und Priming bislang nur indirekte Rückschlüsse aus den Messungen möglich sind. Totalreflexionsfluoreszenz-Mikroskopie (TIRFM) ermöglicht die Echtzeitvisualisierung von fluoreszenten Partikeln mit einem großen Signal-Rausch-Verhältnis, weshalb sich TIRFM für die direkte Untersuchung des Verhaltens von fluoreszenzmarkierten Vesikeln direkt vor dem Fusionsschritt eignet.

In der vorliegenden Studie wurden „large dense-core vesicles“ (LDCVs) in bovinen chromaffinen Zellen durch Überexpression von fluoreszenten Fusionsproteinen markiert und die Bewegungen der Vesikel über die Zeit mittels TIRFM beobachtet. Die Bewegungen der LDCVs wurden mit der in dieser Arbeit vorgestellten „caging diameter“ Analyse untersucht, welche eine Quantifizierung der dynamischen Änderungen des Bewegungsverhaltens von Vesikeln erlaubt. Dabei wurden verschiedene Typen von Bewegungsformen identifiziert und die Vesikel entsprechend in a) unbewegliche Vesikel, b) beschränkt bewegliche Vesikel, c) beschränkt bewegliche und unbewegliche Vesikel, d) Vesikel mit gerichteter Bewegung und e) Vesikel mit gemischten Bewegungsmustern klassifiziert.

Aus früheren Untersuchungen war bekannt, dass die Vesikel in chromaffinen Zellen beim Erreichen der Plasmamembran dort immobilisieren und diese immobilen Vesikel bevorzugt sekretiert werden. Als zugrundeliegender molekularer Mechanismus wurde angenommen, dass während des Primingschrittes der SNARE-Komplex zwischen Vesikel und Plasmamembran ausgebildet und das Vesikel dadurch an der Plasmamembran verankert wird. Aus dieser Modellvorstellung ergibt sich, dass Priming zu einer Immobilisierung der Vesikel führen sollte. In dieser Arbeit wurden daher den als unbeweglich klassifizierten Vesikeln der geprimte Zustand und den beschränkt beweglichen Vesikeln der gedockte ungeprimte Zustand zugeordnet. Zur Überprüfung dieser Einordnung wurde das Priming durch Behandlung der

bovinen chromaffinen Zellen mit Phorbol ester oder durch Überexpression des Primingfaktors Munc13-1 erhöht und die Veränderung der Vesikelbeweglichkeit analysiert. Dabei wurde festgestellt, dass der Anteil an unbeweglichen Vesikeln im Vergleich zu Kontrollzellen erhöht ist. Da Phorbol ester-Behandlung sowie Munc13-1-Überexpression lediglich die Zahl der geprimten Vesikel erhöhen und nur eine Zunahme der Anzahl unbeweglicher Vesikel beobachtet wurde, lässt sich daraus schließen, dass es sich bei den unbeweglichen Vesikeln tatsächlich um geprimte Vesikel handelt. Es ist daher davon auszugehen, dass es sich bei den gedockten, ungeprimten Vesikeln um die beobachteten beschränkt beweglichen Vesikel handelt, während Vesikel mit gerichteter Bewegung den weder gedockten noch geprimten Vesikeln des „depot pools“ zugeordnet werden können.

Zur weiteren Überprüfung dieser Hypothese wurde die Ausbildung des SNARE-Komplexes und damit das Priming von Vesikeln durch Überexpression der leichten Kette von Tetanusneurotoxin verhindert und die Auswirkung auf die Beweglichkeit der Vesikel untersucht. Die leichte Kette von Tetanusneurotoxin ist der enzymatisch aktive Teil, welcher das SNARE-Protein Synaptobrevin proteolytisch spaltet und dadurch die Ausbildung des SNARE-Komplexes zwischen Vesikel und Plasmamembran verhindert. Die Analyse der Vesikelbeweglichkeit zeigte eine Erhöhung der Beweglichkeit. Der Anteil an unbeweglichen Vesikeln war verringert, ebenso der Zeitanteil, welchen Vesikel im immobilen Zustand verbrachten. Dagegen war die Verweildauer der Vesikel im beschränkt beweglichen Zustand erhöht. Dies bestätigt die Hypothese, dass das Priming von Vesikeln mit einer Verringerung der Vesikelbeweglichkeit durch die Ausbildung des SNARE-Komplexes einhergeht.

Abbreviations

α -SNAP	α -Soluble NSF Attachment Protein
ATP	Adenosine Triphosphate
BCC	Bovine Chromaffin Cells
BHK	Syrian Hamster Kidney
BoNT	Botulinum Toxin
BSA	Bovine Serum Albumin
BPB	Bromophenolblue
<i>C. elegans</i>	<i>Caenorhabditis elegans</i>
C	Caged
CA	Catecholamines
CD	Caging Diameter
CAPS	Calcium-dependent activator protein for secretion
cAMP	cyclic adenosine monophosphate
dATP	Deoxyriboadenosine Triphosphate
DNA	Deoxyribonucleotide
DAG	Diacyl Glycerol
DEPC	Diethylpyrocarbonate
DMSO	Dimethylsulphoxide
D	Directed
DTT	1,4-Dithiotheritol
DMEM	Dulbecco's Modified Eagle's Medium
EM	Electron microscope
ER	Endoplasmic Reticulum
ECL	Enhanced chemoluminescence
EDTA	Ethylene Diamine Tetra-Acetic Acid
FFT	Fast Fourier Transform
FCS	Fetal Calf Serum
Fig	Figure
GA	Golgi Apparatus
GFP	Green Fluorescent Protein
HC	Heavy Chain
HEPES	4-(2-hydroxyethyl)-1-piperazineethanesulfonic acid
I	Immobile
IC	Immobile-Caged

IRES	Internal Ribosome Entry Site
LDCV	Large dense-core vesicle
LC	Light Chain
MSD	Mean Square Displacement
M	Mixed
mRFP	monomeric Red Fluorescent Protein
MHD	Munc Homology Domain
MOPS	4-Morpholinepropanesulfonic acid
NGS	Normal Goat Serum
NSF	N-ethylmaleimide sensitive factor
PMA	Phorbol-12-myristate-13-acetate
PBS	Phosphate Buffered Saline
PM	Plasma Membrane
PCR	Polymerase Chain Reaction
PV	Polyvirus
PKA	Protein kinase A
PKC	Protein kinase C
RRP	Readily Releasable Pool
RNA	Ribonucleic acid
RNase	Ribonuclease
RT	Room Temperature
SEM	Standard Error of Mean
SCV	Small Clear Vesicle
SFV	Semliki Forest Virus
SM	Sec1/Munc18 family
SNAP-25	Synaptosome Associated Protein of 25 kD
SNARE	Soluble NSF Attachment Protein Receptor
TeNt	Tetanus Toxin
TIRFM	Total Internal Reflection Fluorescence Microscopy
UPP	Unprimed Pool
VAMP	Vesicle Associated Membrane Protein

1. Introduction

1.1. Secretion: an essential process

The human brain is an organ which stores, computes, integrates and transmits information to all parts of the body. The information travels from one neuron to another across the synapse when neurotransmitter molecules are released from the presynaptic terminal by a process called exocytosis. Exocytosis is the fusion of intracellular transport vesicles with the plasma membrane resulting in either the release of their content extracellularly (regulated exocytosis) or their addition to the plasma membrane (constitutive exocytosis). Constitutive exocytosis allows addition of integral plasma proteins to the plasma membrane for the maintenance of the membrane's function. Regulated exocytosis allows controlled release of membrane-impermeable substances. The best known form of regulated exocytosis is the release of neurotransmitters at the synaptic cleft via fusion of synaptic vesicles with the plasma membrane (PM) of the neuron. Regulated exocytosis of neurotransmitters occurs in response to a local increase of the calcium concentration resulting from an action potential; this process occurs in less than 1 ms. Neurotransmitters in the synaptic cleft then bind to specific receptors on the postsynaptic neuron to elicit specific responses. Neurotransmitters are contained in synaptic vesicles that are called small clear vesicles (SCVs). Another type of vesicle exists which is called the large dense core vesicle (LDCV). Neurons can contain both SCVs and LDCVs (De Potter et al. 1997). Some endocrine and neuroendocrine cells contain LDCVs which secrete their content into the intracellular space by regulated exocytosis. Pancreatic β -cells secrete insulin via LDCVs into the bloodstream via LDCVs to control several metabolic processes including glucose level in the blood. Another type of cell showing regulated exocytosis is the neuroendocrine chromaffin cell in the adrenal medulla which releases adrenaline and noradrenaline, via LDCVs, into the blood in response to stress or danger situations (fight or flight). These are only a few examples of cells that possess a mechanism for regulated exocytosis. Due to the variety of cells

possessing regulated exocytosis and the importance of this process to maintain normal biological functions, it is imperative to understand the mechanisms underlying exocytosis.

1.2. Chromaffin cells: A model of regulated exocytosis.

Neurons consist of a cell body, an axon and one or more dendrites. The distal end of the nerve forms a synapse with the adjacent cell, where a 50 nm wide synaptic cleft separates the presynaptic terminal from the target cell. Neurons have a membrane potential of about -80 mV. When an action potential is initiated, voltage-dependent Na⁺-channels open and Na⁺ flows into the cell, depolarizing the cell. The action potential propagates in the direction of the nerve terminal and when it reaches it, the depolarization causes voltage-gated Ca²⁺-channels to open. The resulting increase of intracellular Ca²⁺ concentration causes vesicles to fuse with the plasma membrane and release their neurotransmitter molecules into the synaptic cleft. These molecules diffuse to the postsynaptic membrane and bind to specific receptor molecules present on the postsynaptic cell, thereby eliciting a specific response (Siegelbaum and Kandel 1991).

For studying presynaptic function and neurotransmission, the neuron itself is the appropriate cell and the most often used method to study neurotransmission is to measure postsynaptic responses. However, this is an indirect method and has shortcomings. First, the number of receptors on the postsynaptic membrane is limited, thus when neurotransmitter saturates these receptors, additional neurotransmitters released will not be observed in the postsynaptic response. Second, the response measured at the postsynaptic side arrives several milliseconds after the actual fast release of the neurotransmitters. In order to circumvent these problems, a method to measure directly release of neurotransmitters is required. However, presynaptic terminals in mammalian synapses are usually quite small and very difficult to access with electrodes or other probes. Several solutions have been devised to circumvent this problem: the study of giant synapses such as the lamprey giant reticulospinal synapse (Low et al. 1999), the goldfish retinal

bipolar neurons (Heidelberger et al. 1994), the glutamatergic calyx of Held giant synapse in the brainstem (Borst et al. 1995) and the ribbon-type synapses of inner hair cells (Beutner et al. 2001). Another solution was offered by Rosenmund and Stevens (1996). They prepared a neuronal culture in which single neurons grow and form synapses with themselves (autaptic culture). In this way both excitatory and inhibitory synapses can be studied practically from all regions of the brain. Another problem to overcome is the difficulty of measuring and controlling presynaptic Ca^{2+} concentrations in most neurons (Schneppenburger and Neher 2000). Therefore another system has been extensively used: the adrenal chromaffin cell (Voets et al. 2000; Rettig et al. 2002). Regulated exocytosis can be measured with different methods with high time resolution in chromaffin cells and the experimental conditions can be controlled to a great extent.

Neurons and chromaffin cells originate from the same precursor cells during embryonic development. These precursor cells differentiate into neurons if they are induced by fibroblast growth factor and nerve growth factor. When they are induced by glucocorticoids they differentiate into chromaffin cells (Cole et al. 1995). Chromaffin cells migrate from the neural crest to the adrenal medulla during embryonic development. The adrenal medulla represents the inner part of the adrenal glands (a pair of endocrine organs situated cranially to the kidneys). The adrenal glands secrete steroid hormones (mineralocorticoids, glucocorticoids as well as androgens) from their cortices and catecholamines (CA) from the medulla, into the blood stream. Dopamine, adrenaline and noradrenaline are called catecholamines because they all contain a catechol (hydroxyl benzene) and an amino group. These molecules are also synthesized in the brain and are used for neurotransmission in neurons. Chromaffin cells can be separated into adrenaline secreting and noradrenaline secreting cells. Additionally, there seems to be evidence for a third type which secretes both adrenaline and noradrenaline (Cahill et al. 1996). The adrenal medulla is a part of the sympathetic nervous system. The stimulus for CA release from chromaffin cells originates from sympathetic nerve endings which release acetylcholine. Acetylcholine, an important neurotransmitter of the peripheral nervous system,

causes membrane depolarization and results in the opening of voltage-gated Ca^{2+} channels. The resulting Ca^{2+} influx triggers exocytosis.

Chromaffin cells share common features with neurons such as the capability to generate action potentials, the presence of fast synchronized transmitter release -although the release time constant was found to be 150-1000 ms (Kasai 1999)- and expression of the major proteins involved in exocytosis (Kits and Mansvelter 2000). However, the anatomy of the chromaffin cell is different from that of the neuron. Chromaffin cells are spherical (Fig. 1) and do not exhibit specific zones for vesicle release (active zones) such as those present in neurons. Also, some proteins that are essential for exocytosis in neurons are absent in chromaffin cells such as Munc13-1 (which will be mentioned in a later chapter). Nevertheless, studies of the proteins involved in regulated exocytosis in the chromaffin cell have allowed a better understanding of the molecular mechanisms underlying exocytosis.

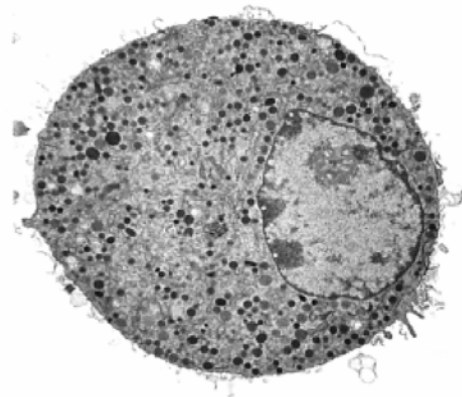


Fig 1: EM of a chromaffin cell: it contains 20.000 to 30.000 vesicles that store adrenaline or noradrenaline. The vesicles darken and become electron dense when treated with several chromium salts whereby their names: large dense core vesicles.

1.3. Molecular changes prior to membrane fusion in chromaffin cells

Before a vesicle fuses with the plasma membrane, it has to undergo a number of molecular changes (Fig. 2). Vesicles originate in the endoplasmic reticulum (ER) and mature in the Golgi apparatus (GA). They are then loaded with neurotransmitters via transporters already present in the vesicle membrane such as vesicular amine transporter. At this point the vesicle resides in the depot pool. The depot pool is represented by vesicles that are in the cytoplasm, 300 nm away from the PM as visualized by electron microscopy (EM).

Vesicles leave the depot pool, approach the PM and become “docked”. Docked vesicles are located close to the PM (from 0 to 300 nm from the PM as seen in EM). Docking was shown to be a reversible process in neurons and neuroendocrine cells (Oheim et al. 1998; Zenisek et al. 2000). After docking, vesicles must undergo a maturation step called “priming”, which renders them fusion competent. As for docking, priming was shown to be a reversible process (Rettig and Neher 2002).

After a local increase of $[Ca^{2+}]_i$, the primed vesicle fuses with the PM and its content is released in the extracellular space. Much later the membranes of the vesicles which fused with the PM are taken up via endocytosis and the vesicle can either be recycled via several endosomes and finally to the GA or is directly reloaded with neurotransmitters during the kiss and run mechanism (Artalejo et al. 2002).

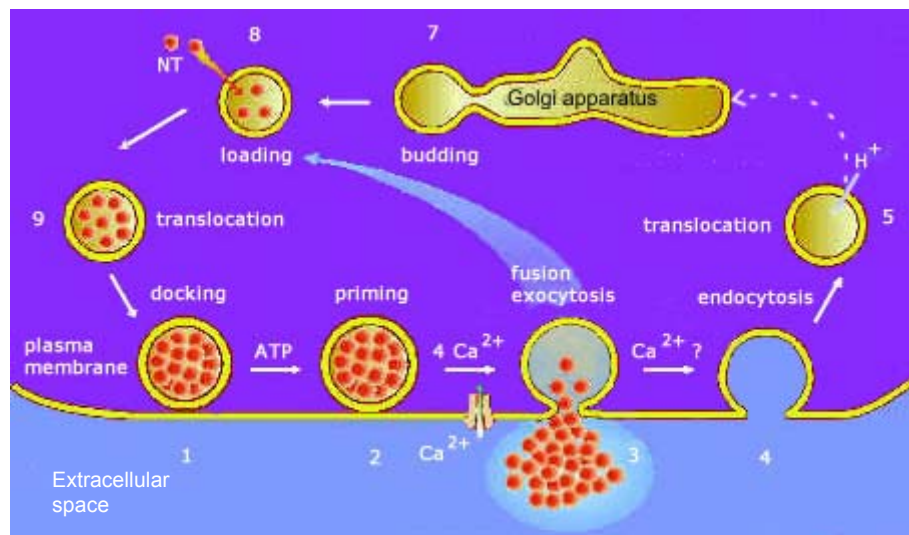
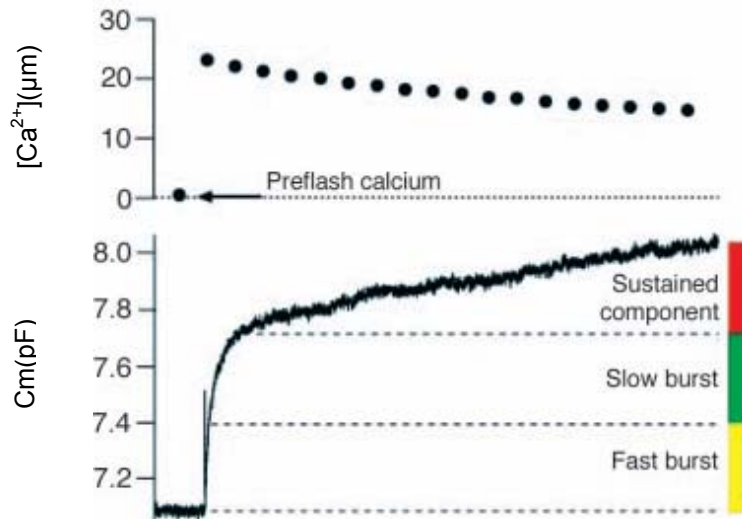


Fig. 2: Secretory vesicle cycle, steps leading to exocytosis. The vesicles are budded from the GA (7), loaded with neurotransmitters (8) then docked to the plasma membrane (1) and primed (2). Upon increase of Ca^{2+} concentration, exocytosis occurs (3). The vesicle is then endocytosed (4), acidified and translocated at a later time to the Golgi apparatus via endosomes to reenter the cycle (5). (Modified from www.uniklinik-saarland.de/physiologie/.)

The sizes of the depot and docked pools have been determined using EM. The docked pool consists of both primed and unprimed vesicles. The size of the primed pool and the kinetics regulating it were determined using membrane capacitance measurements. The PM has electrical properties similar to that of a capacitor. Thus, changes in the capacitance of the cell

reflect the changes in the membrane's surface area. Upon exocytosis, the vesicle membrane is incorporated into the PM, increasing the area of the PM, resulting in an increase in capacitance.

A



B

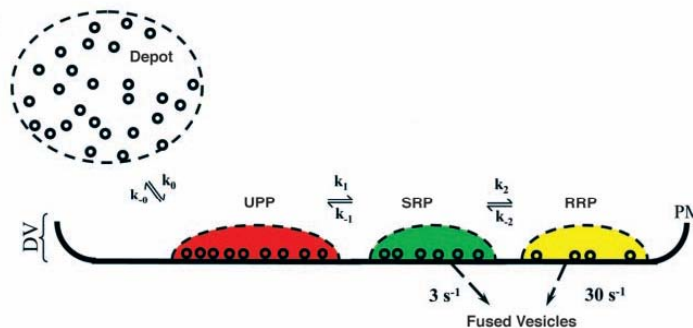


Fig. 3: (A) The response to a step elevation of $[Ca^{2+}]_i$ from 300 nM to 20 μM consists of a triphasic capacitance increase. Membrane capacitance increases in proportion to the number of vesicles that fuse with the plasma membrane. The different components of capacitance response reflect the different pools of vesicles as assigned by the color code. (B) The depot pool contains about 2,000 vesicles. 850 vesicles are morphologically docked and subdivided into the UPP (about 650 vesicles) and the SRP and RRP (Rettig and Neher 2002).

In chromaffin cells, increasing intracellular $[Ca^{2+}]$ using flash photolysis of caged Ca^{2+} lead to an increase in the capacitance of the cell that can be divided into three components (Fig. 3A).

The first two components called together “exocytotic burst” can each be fit with one time constant, the first “fast burst” corresponding to the rate of release of a readily releasable pool (RRP, yellow in Fig. 3) and the second “slow burst” corresponding to the rate of release of a more slowly releasable pool (SRP, green). These two pools correspond to the primed pool. The third and much slower sustained component represents the release of vesicles coming from the docked but unprimed pool (UPP, red) that undergo priming and then fuse. The kinetics of docking and priming (or undocking and unpriming) were calculated from capacitance recording. k_0 and k_{-0} represent the rates of docking and undocking, respectively. k_1 and k_{-1} are the rates of priming and unpriming and k_2/k_{-2} are the rates of turnover between the RRP and SRP.

To date, no method has been developed to obtain direct information about docking and priming kinetics. Therefore, a technique that allows the real-time visualization of the vesicles would be the method of choice to observe the different molecular states of the vesicle over time.

The different processes leading to exocytosis are a result of different molecular events, such as phosphorylation of ATP, Ca^{2+} -binding and conformational changes in the SNARE complex. Various proteins enhance or inhibit the different steps leading to exocytosis (translocation of vesicles, docking, and priming); these will be described in the next chapter.

1.4. Proteins involved in exocytosis

For exocytosis to occur, the lipid bilayers of the vesicle and the plasma membrane have to fuse. Therefore the repulsive forces of the opposing polar headgroups need to be overcome (Oberhauser et al. 1992). These forces may be overcome by fusion-mediating proteins. Many proteins involved in membrane fusion have been identified and have been found to consist of groups of conserved proteins (Jahn et al. 2003). Nevertheless, the mechanisms underlying the function of many of these proteins are still unknown. The main players in exocytosis are the SNARE proteins.

SNARE proteins are a large protein superfamily consisting of more than 60 members which contain domains that are highly conserved from yeast to mammals (Pelham 1999). The primary role of SNARE proteins is to mediate fusion of cellular transport vesicles with the PM or with a target compartment (such as a lysosome). SNAREs can be divided into two categories: *vesicle-* or *v-SNAREs*, which are incorporated into the membranes of transport vesicles during budding, and *target-* or *t-SNAREs*, which are located in the membranes of target compartments. Recent classification however takes account the structural features of the SNARE proteins and divides them into R-SNAREs and Q-SNAREs respectively (Chen and Scheller 2001). Both classifications (v/t and Q/R) are widely used. SNAREs are small, abundant and mostly plasma membrane-bound proteins. Although they vary considerably in structure and size, all share a segment in their cytosolic domain called a *SNARE motif* that consists of 60-70 amino acids that are capable of reversible assembly into tight, four-helix bundles called "*trans*"-*SNARE complexes*. The best-studied SNAREs are the neuronal SNAREs. These SNAREs are the targets of bacterial neurotoxins responsible for botulism and tetanus. In neurons, the readily-formed metastable "trans" complexes are composed of three SNAREs: syntaxin 1 and SNAP-25 resident in cell membrane (t-SNAREs) and synaptobrevin (a v-SNARE; also referred to as vesicle-associated membrane protein or VAMP) anchored in the vesicular membrane. Syntaxin and synaptobrevin are anchored in their respective membranes by their C-terminal domains, whereas SNAP-25 is tethered to the PM via several cysteine-linked palmitoyl chains (Washbourne et al. 2001).

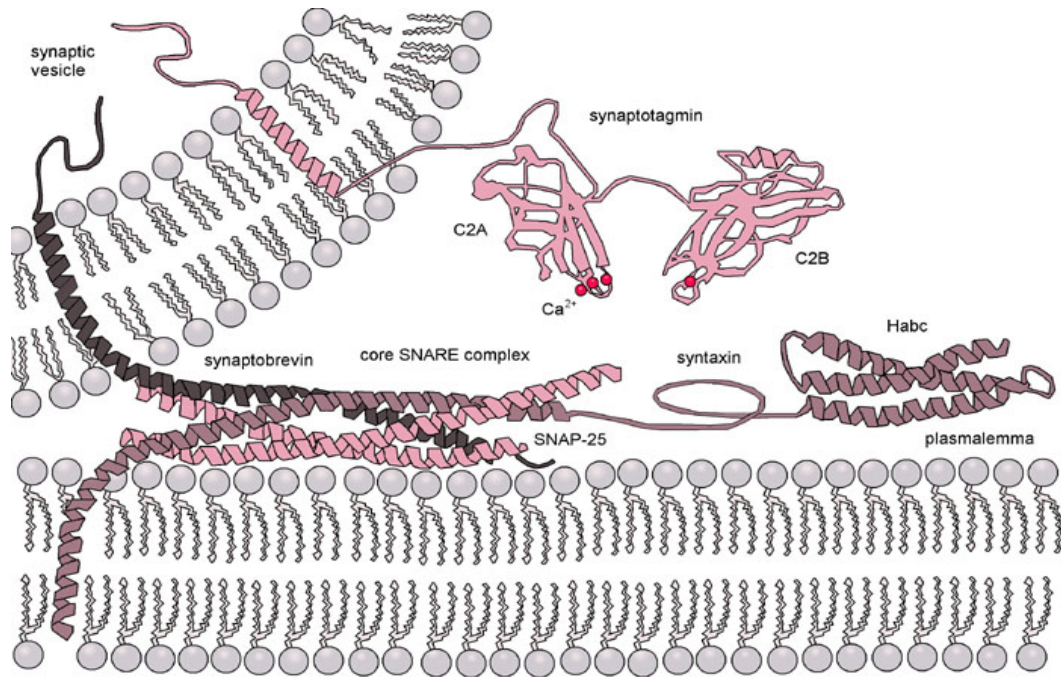


Fig. 4: Molecular machinery driving exocytosis. The SNARE complex is formed by four α -helices contributed by synaptobrevin, syntaxin and SNAP-25. Synaptotagmin serves as a Ca^{2+} sensor and regulates intimately the SNARE zipping. (Reproduced from www.en.wikipedia.org/)

The core SNARE complex is composed of four α -helices in a bundle, where one α -helix is contributed by syntaxin-1, one α -helix by synaptobrevin and two α -helices are contributed by SNAP-25 (Bennett et al. 1993; Sollner et al. et al. 1993; Hanson et al. 1997; Sutton et al. 1998; Lonart et al. 2000). The t-SNAREs have been shown to be present in distinct microdomains or clusters, the integrity of which is essential for the exocytotic competence of the cell.

Prior to fusion, the SNARE proteins involved combine to form a “*trans*”-SNARE complex through an intermediate complex composed of SNAP-25 and syntaxin-1, which later accommodates synaptobrevin-2 (Bennett and Scheller 1993; Sollner et al. 1993; Hanson et al. 1997; Sutton et al. 1998; Lonart and Sudhof 2000). Assembly of the SNAREs into the “*trans*” complexes likely bridges the gap between the apposed lipid bilayers of membranes belonging to the cell and the secretory granule, bringing them in proximity and inducing their fusion. During fusion, the membranes merge and SNARE proteins involved in complex formation after fusion are then referred to as a “*cis*”-SNARE complex, because they now reside in a single membrane. The influx of calcium into the cell triggers the completion of the

assembly reaction, which is thought to be mediated by an interaction between the putative calcium sensor, synaptotagmin, with membrane lipids and/or the partially assembled SNARE complex. According to the "zipper" hypothesis (Hanson et al. 1997; Hay and Scheller 1998), complex assembly starts at the N-terminal parts of SNARE motifs and proceeds towards the C-termini that anchor interacting proteins in membranes. The disassembly of the SNARE complex is catalysed by NSF and α -SNAPs to recycle the SNAREs for another round of fusion. Before fusion, the trans- complex is proposed to change from a loose into a tight state (Xu et al. 1999). This would be consistent with the presence of SRP, reflecting the loose state, from which the vesicles are able to fuse at lower rates. The tight state would support the fast exocytosis from the RRP (Xu et al. 1999; Rettig and Neher 2002)

As mentioned above the neuronal SNARE proteins are highly sensitive to clostridial neurotoxins. These neurotoxins share common features: they weigh 150-kD and are made up of two parts, a 100-kD heavy chain (HC) and a 50-kD light chain (LC). The HC mainly serves as the delivery system for the LC component. The LC is the protease component of the toxin and cleaves a specific SNARE protein when it is not in the SNARE complex. Botulinum toxin (BoNt) is produced by the bacterium *Clostridium botulinum* and has seven serologically distinct toxin types from A to G. BoNt/A and E cleave SNAP-25, BoNt/C cleaves syntaxin while BoNt/B, D, F and G cleave synaptobrevin (Fig. 5). This blocks exocytosis of neurotransmitters and leads to total paralysis (Breidenbach and Brunger 2005).

Tetanus toxin (TeNT) is produced by the vegetative spore of *Clostridium tetani* in anaerobic conditions. The LC cleaves synaptobrevin I and II and cellubrevin (Schiavo et al. 2000). This cleavage prevents synaptobrevin from forming the SNARE complex and exocytosis is blocked (Schiavo et al. 2000).

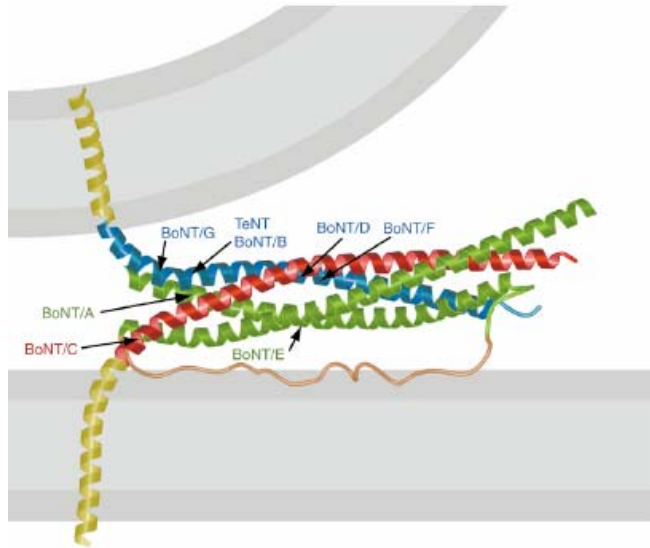


Fig. 5: Clostridial neurotoxins. Each toxin specifically cleaves a SNARE protein (Sutton et al. 1998).

1.5. Proteins involved in docking

Membrane capacitance measurements cannot give information about docking, thus not much is known about the proteins that mediate this step. Additionally, some proteins seem to have more than one function (docking and priming) or even opposite ones (priming and unpriming). One of these proteins is Munc18-1.

Munc18-1 is a member of the sec1/Munc18 (SM) family. It is expressed at synapses and binds to the N-terminal Habc domain of syntaxin1 outside the SNARE motif, thereby stabilizing the closed conformation of syntaxin1 and preventing its interaction with VAMP and SNAP-25 (Dulubova et al. 1999). Thus if Munc18-1 were deleted, secretion would increase. Yet, the opposite was observed in chromaffin cells (Voets et al. 2001). It was then suggested that Munc18-1 has a chaperone function by stabilizing syntaxin at the PM (Toonen et al. 2005).

However, it is unclear how the interaction of Munc18-1 with syntaxin mediates docking. Hence, other interaction partners might be involved such as Mint and DOC2 (Brose et al. 2000; Schutz et al. 2005). These interactions seem to be important for docking.

The Rab3-RIM complex may also mediate docking. It was shown that overexpression of Rab3s in PC12 cells led to an increase in the number of docked vesicles (Martelli et al. 2000) whereas its depletion led to a reduction in secretion (Schluter et al. 2004; Schluter et al. 2006). Similarly, a RIM-1

knockout leads to a decrease in the number of docked vesicles (Schoch et al. 2002; Calakos et al. 2004). Finally, it is possible that docking is coordinated by other proteins such as bassoon and piccolo (Garner et al. 2000).

1.6. Proteins involved in priming

Several factors affect priming whether by increasing the rates of priming (k_1 and/or k_2 , fig. 3) or by decreasing the rates of unpriming (k_{-1} and/or k_{-2} , fig. 3). The complexins, a family consisting of two isoforms, complexin I and II, modulate the priming rate. Genetic deletion of complexin I and II greatly decreased release efficiency. Release in hippocampal neurons could be rescued by increasing the extracellular Ca^{2+} concentration (Reim et al. 2001). This result was also obtained in mast cells following siRNA knockdown of complexin II (Tadokoro et al. 2005). In contrast, it has been found that overexpression of complexin in chromaffin cells led to a reduction in secretion and to a faster time course of single secretion events (Archer et al. 2002). So it might be possible that complexin plays also a role in fusion pore opening. Hence, this protein seems to have more than one function and electrophysiological methods have not allowed the determination of its precise function.

Protein kinase A (PKA) was shown to promote priming by decreasing k_{-1} . When the intracellular Ca^{2+} concentration increases, the production of cyclic adenosine monophosphate (cAMP) increases which in turn activates PKA. It was shown that constitutive PKA activity results in the phosphorylation of SNAP-25, a process necessary for the maintenance of a large number of vesicles in the primed pool (Nagy et al. 2004).

Protein kinase C (PKC) was shown to decrease k_{-1} thus promoting priming. It is activated by an increase in the intracellular Ca^{2+} concentration, since Ca^{2+} binds to PKC's C2 domains. Also, diacyl glycerol (DAG, a secondary messenger) and phorbol esters such as phorbol myristate acetate, that imitate DAG in its action, activate PKC (Newton 1997). Both DAG and phorbol esters bind to the C1 domain of PKC and lead to its translocation to the plasma membrane. PKC may act through phosphorylation of SNAP-25 at Ser 187 (Nagy et al. 2002).

The Munc13's are a family of proteins consisting of Munc13-1, -2, -3 and -4. Munc13's appear to be required for priming (Aravamudan et al. 1999; Augustin et al. 1999; Richmond et al. 1999; Brose et al. 2000). They are the mammalian homologues of unc-13, a large family of proteins originally found in *C. elegans* (Brenner 1974). Munc13's structure is highly conserved.



Fig. 6: Munc 13-1 Domain structure. For detailed explanation, see text.

They contain two “Munc Homology Domains” (MHD), a C1-domain and two (Munc13-1, -2 and -3) or three (Munc13-4) C2-domains. The latter function as Ca^{2+} /phospholipids-binding domains. The C1-domain is functionally similar to the C2-domain of PKC which is the DAG binding domain (Betz et al. 1998; Ashery et al. 1999; Rhee et al. 2002). Like PKC, Munc13's are displaced to the plasma membrane after binding DAG and its synthetic analogues, the phorbol esters. Munc13-1 is thought to function by interacting with syntaxin1. This interaction appears to displace Munc18 from the N terminus of syntaxin1 and thus allows syntaxin1 to interact with SNAP25 and synaptobrevin. Then core complex assembly can occur (Brose et al. 2000). Recently, it has been shown that point mutations in the MHDs and in the C-terminal region of the C2-domain binding regions to syntaxin1, reduce the function of Munc13 (Madison et al. 2005; Stevens et al. 2005). The Munc13 isoforms also contain a calmodulin binding site. The formation of a calmodulin/Munc13 complex may allow a Ca^{2+} sensing/effector which allows modulation of synaptic vesicle priming and synaptic efficacy in response to a change of $[\text{Ca}^{2+}]_i$ (Junge et al. 2004). For example, during sustained synaptic activity -thus high $[\text{Ca}^{2+}]_i$ -, Munc13's efficacy in keeping syntaxin 1 in its open conformation may be enhanced through its binding to calmodulin. Hence, the Calmodulin/Munc13 complex could be one molecular target of Ca^{2+} action during sustained synaptic activity and thus mediate short term plasticity (Junge et al. 2000), which is dependent on residual $[\text{Ca}^{2+}]_i$ (Zucker 1999).

In chromaffin cells, overexpression of Munc13-1 nearly tripled the amount of secretion and significantly increased the size of the primed pool (Ashery et al. 2000). However, Munc13-1 was not detected in chromaffin cells (Ashery et al. 2000) and the amount of secretion from chromaffin cells of Munc13 triple-knockout mice was similar to that of wild type mice (Stevens and Rettig, unpublished results). Therefore, it is unclear if Munc13-1 plays a role in priming LDCVs in chromaffin cells (the role of Munc13-4 for example needs to be elucidated) or if other priming factors are responsible for priming in chromaffin cells. Calcium-dependent activator protein for secretion (CAPS) was also considered to be a priming factor (Wassenberg and Martin 2002). However, it has recently been shown that CAPS is involved in the loading of these vesicles with neurotransmitters (Speidel et al. 2005). Another possibility would be that priming is a constitutive process in chromaffin cells.

On the other hand, in neurons, Munc13-1 is considered the priming factor par excellence. It was indeed shown by Augustin et al. (1999) that in Munc13-1 knock-out mice, there was a 90% reduction of readily releasable vesicles and evoked transmitter release in excitatory neurons releasing glutamate.

1.7. Total internal reflection fluorescence microscopy (TIRFM)

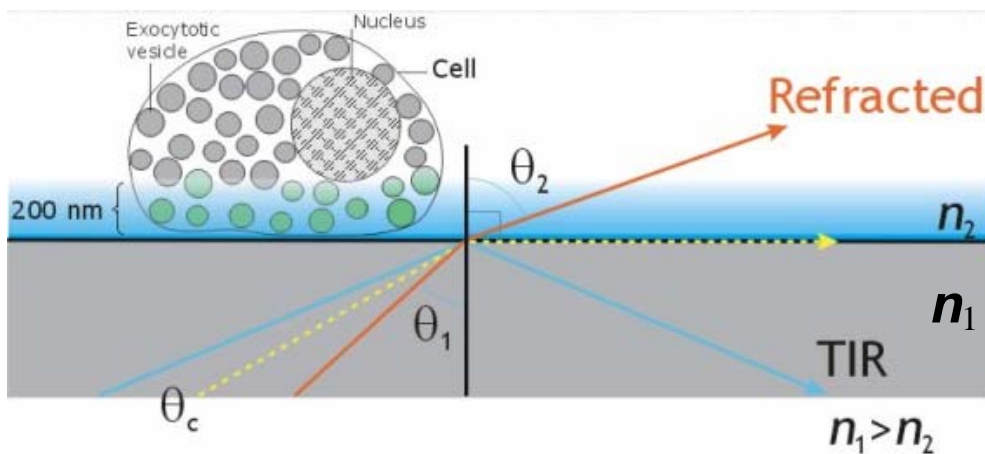
Although a large number of agents that affect priming are now known, no method has allowed the direct observation of the priming event or the differentiation between docked and primed vesicles.

Several imaging techniques were developed in recent years to visualize dynamic changes occurring in living cells. TIRFM is one of them. It relies on the fact that light travels differently in two media with different refractive indices.

When the light hits the interface between two different media it is refracted into the second medium at an angle that is different from the incident angle according to Snell's law: $n_1 \sin \theta_1 = n_2 \sin \theta_2$, where n_1 and n_2 are the refractive indices of the two media and θ_1 and θ_2 are the angles of incidence and refraction respectively (Fig. 7A). When the incident angle reaches a critical

angle, light is totally refracted in the interface. The critical angle depends on the ratio between the refractive indices: $\theta_c = \sin^{-1}(n_2/n_1)$ (Fig. 7A). Beyond this angle all light is reflected. However, some light escapes this reflection and extends in the z direction thus creating a thin electromagnetic field. The strength of this field, also called evanescent field, decreases exponentially with increasing penetration depth and extends only a few hundred nanometers into the second medium (having the lower refractive index) (Fig. 7B).

A



B

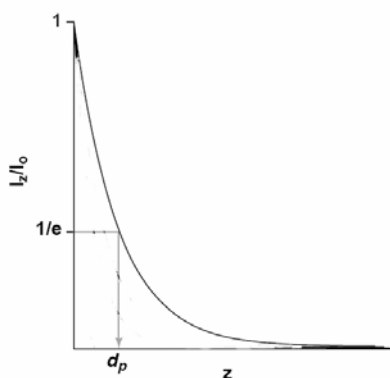


Fig. 7: Principle of TIRFM. (A) Only granules close to the evanescent wave (blue strip) light up. For more details, see text. (B) Intensity (I_z/I_o) decays exponentially with increasing penetration depth (d_p).

The main advantage of TIRFM over epifluorescence and confocal microscopy is the illumination of only a thin section of the specimen whereas the rest of the specimen is not illuminated. Due to this, no background fluorescence is observed and we can obtain pictures of labeled particles with a very high signal-to-noise ratio (Almers et al. 2001; Axelrod et al. 2001; Oheim et al.

2001; Toomre et al. 2001). Also, this decreases the danger of photobleaching. TIRFM is also a relatively inexpensive and low energy consuming technique compared to two-photon microscopy. This method has been used for example to qualify the types of movements made by particles, to visualize exocytosis in real-time recordings and recently to visualize single protein molecules. Therefore TIRFM seems to be the method of choice to visualize fluorescent vesicles as they undergo the different molecular changes (docking, priming, fusion).

1.8. Aim of the work

The molecular changes leading to fusion are processes that are still investigated by many. As mentioned above the number of vesicles in the primed pool was determined by measuring the capacitance increase in the exocytotic burst and calculating how many vesicles this increase corresponds to. Also the rates of docking and priming were determined by using fits to the different components of the triphasic capacitance increase. Still, membrane capacitance measurements do not give direct information on priming and docking, thus it is necessary to develop a method that allows the real-time observation of these processes. TIRFM should be the method of choice to visualize LDCVs as they undergo changes from one molecular state to the other.

Several groups have been able to identify different types of movements of vesicles. Oheim (2001) showed that vesicles could be immobile, restricted in motion or could have a directed motion.

Furthermore, studies (Steyer et al. 1997; Oheim et al. 1999) have shown that as vesicles docked to the PM, their mobility was reduced, as compared to their mobility when they were further away from the PM. This is consistent with the "zipper" hypothesis (Hanson et al. 1997; Hay and Scheller 1998), which states that SNARE complex assembly results in the attachment of the vesicle to t-SNAREs via v-SNAREs which anchors the vesicle to the PM (Fig. 8). Yet no serious attempt has been made to assign these different types of motion to the distinct molecular states.

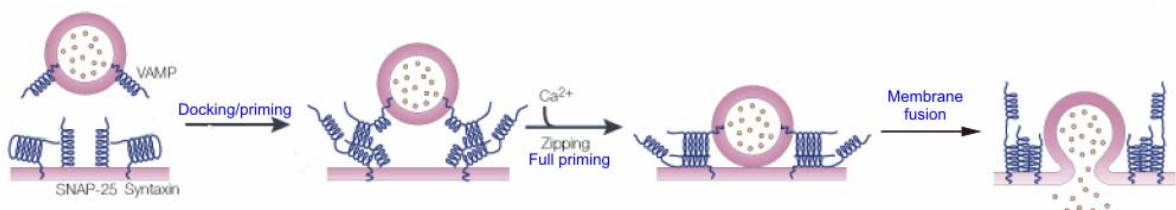


Fig. 8: Zipper hypothesis. The vesicle docks on the PM then undergoes the first priming steps when the SNARE complex starts to form. Upon full priming and zipping of the SNARE proteins, the vesicle is tightly attached to the PM and ready to fuse. Upon local increase in $[Ca^{2+}]_i$, exocytosis occurs (modified from Chen and Scheller 2001).

We propose a model where, as the SNARE is assembled during priming, the vesicle becomes tightly attached to the PM and therefore is not able to move freely.

To verify this hypothesis, I specifically promoted priming using two independent methods:

1- Treating bovine chromaffin cells with phorbol myristate acetate (PMA) which was found to increase the pool of primed vesicles without affecting the size of docked vesicles (Gillis et al. 1996; Smith et al. 1998).

2- Overexpression of Munc13-1 which was found to triple the secretion in chromaffin cells by increasing the size of the RRP without affecting the size of docked but unprimed vesicles (Ashery et al. 2000).

To confirm our observations about priming, I used a virus containing TeNT-LC-GFP to prevent the priming reaction and I expected to observe an opposite effect to that observed in the primed cells.

To visualize the LDCVs, I stained bovine chromaffin cells with neuropeptide Y fused with the monomeric red fluorescent protein (NPY-mRFP). NPY was found to be specifically targeted to LDCVs (Nagai et al. 2002). To track the vesicles, we used a homemade tracking program and a new method of analysis was devised to allow the observation of the dynamic changes that the vesicle is undergoing over time as opposed to the analysis of the Mean Square Displacement, which allows only an overall description of the mobility.

I also ascertained that exocytosis measured by TIRFM is similar to exocytosis measured by membrane capacitance recordings.

Using these different protocols of priming and unpriming, my aim is to distinguish between docked and primed vesicles using their mobilities as a tool of differentiation.

2. Materials and Methods

2.1 Materials

2.1.1 Reagents

Acetic acid	Roth
Agarose for DNA electrophoresis	Roth
Agarose for RNA electrophoresis	Sigma
Albumin	Sigma
2-Amino-2-(hydroxymethyl)-1,3-propantriol (Tris)	Roth
Aprotinin	Sigma
L-aspartic acid	Sigma
Bovine serum albumin (BSA)	Sigma
Bromphenolblue (BPB), sodium salt	Serva
Cesium hydroxide	Sigma
Chloroform	Fluka
dATP	Roth
dCTP	Roth
dGTP	Roth
DMEM (Cat no. 31966-021)	Invitrogen
Dithiotreitol (DTT)	Sigma
D-Glucose	Merck
Diethylpyrocarbonate (DEPC)	Sigma
DNase	Roche
ECL reagent	GEhealthcare

EDTA	Sigma
Ethanol	Roth
Ethidium bromide	Invitrogen
Fetal calf serum (FCS)	Invitrogen
Formaldehyde 37%	Sigma
Formamide	Sigma
Glutamic acid	Sigma
Glycerol	Sigma
H ₂ O	Sigma
ITS-X	Invitrogen
L-cysteine	Sigma
4-Morpholinepropanesulfonic acid (MOPS)	Sigma
Mounting medium	Vectashield
Normal goat serum (NGS)	Invitrogen
NE-buffer 10x	Biolabs
N-(2-Hydroxyethyl)-1 piperazine-N'-(ethanesulfonic acid) (HEPES)	Sigma
Nitrocellulose membrane (0.2 µm pore size)	Roth
OptiMem1	Invitrogen
PBS	Invitrogen
10x PCR Buffer	Sigma
Penicilline/Streptomycine	Invitrogen
Phenol for DNA purification	Sigma
Phenol for RNA purification	Roth
Phorbol 12-myristate 13-acetate (PMA)	Sigma
2-Propanol	Roth
RNase Inhibitor	Roche

Skimmed milk powder	Naturaflor®
Tetrodotoxin	Sigma
Triton® X-100	Serva
Trypsin-EDTA 10x	Invitrogen
Trypsin Inhibitor	Sigma
Tryptosephosphate	Invitrogen
Whatman-3 MM-paper	Whatman
Xylen cyanol FF	Sigma

All other chemicals were ordered from Merck

2.1.2 Enzymes

Chymotrypsin	Sigma
Collagenase CLS	Biochrom AG
Proteinase K	Qiagen
RedTaq-Polymerase	Sigma
Trypsin	Invitrogen
SpeI	Biolabs
SP6-RNA-Polymerase	Roche

2.1.3 Plasmids

The plasmids pSFV1 and pSFV1-PV-IRES were provided by U. Matti (Department of Physiology, Saarland university, Homburg, Germany).

2.1.4 Media and solutions

2.1.4.1 Solutions for chromaffin cell preparation

Locke's

154 mM NaCl

5.6 mM KCl

0.85 mM NaH₂PO₄ x H₂O

2.15 mM Na₂HPO₄ x H₂O

10 mM glucose

pH 7.4 ; ≈ 312 mosm

Collagenase solution

290 U/ml locke's solution.

Inactivating solution

10% FCS in locke's solution.

Medium

for two 6-well plates:

30 ml DMEM

300 µl ITS-X

120 µl Pen./Strep.

→ freshly prepared; 37°C, 9% CO₂

2.1.4.2 Solutions for BHK cell culture/virus generation and activation

OptiMem1 + 2,5%FCS

Tryptosephosphate 100 ml

HEPES 1M 20 ml

FCS 25 ml

Pen. / Strep. 1 ml

filled up with OptiMem1 to 1000 ml

→ sterile/ 4°C

OptiMem1 + 5%FCS

Tryptosephosphat 15 ml

HEPES 1M 3 ml

FCS 7,5 ml

Pen / Strep 150 µl

filled up with OptiMem1 to 150 ml

→ sterile/ 4°C

OptiMem1 without FCS, + 0,2% BSA

OptiMem1 44ml

Tryptosephosphat 5ml

HEPES 1M 1ml

Pen / Strep 50µl

BSA 0,1g

→ sterile/ 4°C

Aprotinin

6 mg/ ml in HBS (aliquots, -20°C)

Chymotrypsin

2 mg/ ml in HBS (aliquots;-20°C)

Trypsin/ EDTA 10x

diluted 1:10 in PBS

DEPC-H₂O 0.1 %

1ml DEPC

in 1l ddH₂O

5x Mops

3,28 g Sodium acetate

20,6 g MOPS

diluted in 800 ml DEPC-H₂O; pH 7.0

+ 10 ml 0.5 M EDTA pH 8.0

filled up with DEPC-H₂O to 1000 ml → sterile filtered; stored in the dark

Loading buffer for RNA gel:

10 ml	5 x MOPS	(1x)
8,5 ml	37%-Formaldehyde	(6,5%)
25 ml	Formamide	(50%)
2,5 ml	Glycerol	(5%)
10 µl	0.5M EDTA pH8	(0,1mM)
0,0125 g	BPB	(0,025%)
2,75 ml	H ₂ O	

→ aliquots ; -20°C

2.1.4.3 Solutions for TIRFM experiments

Ringer: 140 mM NaCl, 2.4 mM KCl, 2 mM CaCl₂, 1 mM MgCl₂, 10 mM Glucose, 10 mM HEPES (pH 7.3)

High K⁺: 52.4 mM NaCl, 90 mM KCl, 3 mM CaCl₂, 10 mM Glucose, 10mM HEPES (pH 7.3)

2.1.4.4 Solutions for whole-cell patch experimentsExtracellular solution:

146 mM NaCl, 2.4 mM KCl, 10 mM HEPES, 1.2 mM MgCl₂, 2.5 mM CaCl₂, 10 mM Glucose and 10 mM NaHCO₃ (pH 7.4).

Pipette solution:

160 mM L-aspartic acid, 1 mM MgCl₂, 2 mM MgATP, 0.3 mM Na₂GTP, 10mM HEPES (pH 7.2).

2.2 Methods

2.2.1 Bovine chromaffin cell preparation

The adrenal glands were obtained from a slaughterhouse and cleaned of all connective tissue with scissors. The glands were perfused with 10 ml Locke's solution through the adrenal vein and put in a shaking water bath for 10 min. This step was repeated 4-6 times until all the blood was washed out of the glands. I then proceeded with the digestion of the glands with Locke's solution containing 290 U/ml collagenase. Each gland was perfused with 10 ml enzyme solution and put in a shaking water bath for 14 min; this step was repeated with the gland positioned on its opposite side. The digestion was then stopped by perfusing the glands with 10 ml 10% FCS, then the glands were cut in two halves to expose the medulla. The medulla was carefully removed with a forceps and transferred to a Petri dish containing a few milliliters of Locke's solution. The medulla was then cleaned of any traces of blood vessels or impurities. The medulla was shredded with scissors and then transferred to a 50 ml falcon tube and completed to 20 ml with Locke's solution. The tissue was gently shaken for 1 min and centrifuged at 700 rpm for 2 min, after which the supernatant was discarded and the tissue was resuspended in Locke's solution, and then dispersed by passing through a nylon mesh. Locke's solution was added to bringing the resulting cell suspension to a final volume of 20 ml. The cell suspension was then centrifuged at 700 rpm for 7 min. After each centrifugation, the resultant supernatant was discarded and the pellet was resuspended in 10 ml of Locke's solution and transferred to a 15 ml falcon tube. The tube was centrifuged 3-4 times at 600 rpm for 5 min and one last time at 300 rpm for 5 min. Each time, the supernatant was discarded and the resultant pellet was resuspended in an appropriate amount of modified DMEM medium. The cells were counted and diluted

so that they could be plated at a density of 3×10^5 cells/ml in modified DMEM medium, kept at 37°C, 9% CO₂ and used 3-5 days after plating.

2.2.2 Protocol for electroporation

For one electroporation, 800 µl of cells in DMEM solution (2.5×10^6 cells/ml) were incubated with 20 µg of DNA for 3 min on ice. The cells were then transferred in 0.4 cm Gene Pulser cuvettes and electroporated with the Gene Pulser II (Biorad) with the following specifications: 230 V and 1000 µF. The cuvette was then kept on ice for 2 min and the cells were allowed to recover in a water bath (37°C) for 10 min. The cells were then carefully transferred into 15 ml falcon tube and centrifuged at 400 rpm for 2 min. The supernatant was discarded and the cells were resuspended in 1.5 ml DMEM solution then plated on 6 well plates.

2.2.3 Protocol for virus generation, activation and infection

For virus infection I used a Semliki forest virus (SFV) which is an alpha virus from the family togaviridae and is a useful tool in heterologous protein production (DiCiommo and Bremner 1998). This virus has been found to successfully infect chromaffin cells (Ashery et al. 1999). The SFV genome is of positive polarity, i.e. it functions directly as mRNA, and infectious particles can be obtained by in-vitro transcription of a full-length cDNA copy of the genome. Advantages of this system are the efficient RNA replication, the relatively late onset of cytopathogenic effects and the broad host range of the SFV. In this work, a modified version of the pSFV1 plasmid containing an internal ribosome entry site from polyvirus was used. This pSFV1-PV-IRES plasmid contains a unique BamHI and BssHII site upstream of the PV-IRES and a unique NruI site downstream. Genes cloned into this plasmid also need a Kozak sequence and start codon.

Electroporation was used when a high density of marked vesicles was needed while virus infection was used to yield a low density of stained vesicles for the tracking experiments. Cells were electroporated with NPY-mRFP.

2.2.3.1 Cultivation of BHK21 cells

The BHK-21 cell line (c-13, ATCC™ccL-10) containing Syrian hamster kidney cell type cells was used for SFV production. BHK cells were cultivated in Opti-Mem1 with

2.5% FCS in 75 cm² cell culture flasks. 80-90 % confluent cells were split routinely using trypsin/EDTA. For splitting, the growth medium was aspirated and the cells were washed once with OptiMem1. Then 6 ml trypsin/EDTA was added and incubated for \approx 1 minute until cells were detached from the bottom. Cells were triturated with the 10 ml pipette for separation. The suspension was put into a falcon tube with stop medium (OptiMem1+ 5% FCS) and centrifuged 3 min at 1300 rpm. Cells were washed with 10 ml OptiMem1 and centrifuged (3 min, 1300 rpm) twice. Then they were counted and the desired cell number was cultivated in a new cell culture flask (37°C, 5% CO₂). For long term storage cells were harvested in a cryoprotectant medium containing DMSO in the cryovials and were frozen in liquid nitrogen.

2.2.3.2 Preparation of viral RNA

The pSFV1 vector contains three unique cloning sites (BamHI, BssHII and NruI). DNA fragments cloned in these sites must encode their own Kozak sequence and an AUG translation initiation site. The cDNA coding for NPY-mRFP (Tsuboi et al. 2003) including a Kozak consensus sequence was subcloned into the BamHI-BssHII site of the pSFV1 polylinker or in the pSFV1-PV-IRES. The cDNA coding for Munc13-1-eGFP (Ashery et al. 2000) and the cDNA coding for TeNt-LC-eGFP (Borisovska et al. 2005), both including a Kozak sequence, were subcloned each into the NruI site of the pSFV1-PV-IRES. Viral RNA was prepared by in-vitro transcription of plasmids pSFV1 coding for SFV non-structural and pSFV-helper2 coding for structural proteins. Following linearization with SpeI, DNA was transcribed in-vitro using the Capscribe SP6 kit (Roche) according to the manual.

2.2.3.2.1 Linearization of DNA

Linearization was carried out at singular SpeI sites downstream of the polyA tail encoded on pSFV1 and pSFV1-PV-IRES. A total volume of 25 μ l containing 3 μ g DNA, 2.5 μ l NE-buffer, 2.5 μ l BSA 10%, 1.5 μ l SpeI and the calculated volume of Sigma H₂O was incubated at 37°C for 1.5 hours. To verify complete linearization, 1 μ l of the DNA diluted in 2 μ l 6xSLB (Loading buffer) and 9 μ l Sigma H₂O was run on a 1% Agarose gel. Reference was 4% λ -DNA Marker (4 μ l Marker+ 2 μ l 6xSLB+9 μ l Sigma H₂O). Electrophoresis was carried out at 80 Volts for 60 minutes. DNA was visualized by UV illumination (312 nm) on the gel documentation system (Phase, Lübeck, Germany).

2.2.3.2.2 In-vitro transcription

Linearized DNA was purified by extraction with phenol-chloroform and ethanol precipitation. The remaining 24 μ l of the restriction digest were vortexed with 176 μ l Sigma H₂O, 200 μ l phenol and 2 drops (\approx 12 μ l) of chloroform. The supernatant was removed after centrifugation (10 min, 14000 rpm) and the residual phenol present in the supernatant was extracted by 200 μ l chloroform. After another centrifugation step (5 min, 14000 rpm) the DNA was recovered from the supernatant by precipitation at -20°C (or 2 hours at -80°C) with 500 μ l ethanol (100%, cold) in the presence of 20 μ l 3M Sodium Acetate. The DNA was pelleted by centrifugation at 14000 rpm for 15-30 min, washed with 500 μ l 70% ethanol and redissolved in 13 μ l of RNase-free water after drying in the dessicator at RT. For transcription, the DNA was mixed with 8 μ l Cap scribe buffer, 1 μ l RNase inhibitor, 2 μ l SP6, 16 μ l Sigma H₂O and incubated for 2 hours at 37°C . Afterwards the DNA template was digested by mixing the transcription reaction with 36 μ l RNase-free water and 4 μ l DNase within 20 minutes at 37°C . The product was purified by extraction with phenol and chloroform as described above for DNA (here phenol for RNA isolation: Aqua Roti phenol pH 4.5-5). Following precipitation the sample was centrifuged 15-30 min at 14000 rpm, 4°C and the pellet was washed twice with cold 70% ethanol, vortexed and centrifuged (14000 rpm, 10min, 4°C). The pelleted RNA was collected, desiccated and dissolved in 20 μ l RNase-free water.

2.2.3.2.3 Quantification of RNA amount by electrophoresis

Agarose gels were prepared by dissolving 0.4 g agarose in 20 ml DEPC-H₂O, heating in a microwave oven, adding 5.3 ml of 5x MOPS buffer and 4.7 ml of 37% Formaldehyde. 1 μ l RNA sample was mixed with 9 μ l loading buffer (20 μ l RNA buffer+5 μ l ethidiumbromide). 3 μ l RNA Ladder was diluted in 8 μ l loading buffer. Both samples were denatured by incubation for 10 minutes at 65° to eliminate secondary structures of the RNA. After loading them on the gel electrophoresis was performed for 10 min at 80 Volts and then 85 min at 100 Volts. The gel was analyzed with the phase gel documentation system and the amount of RNA was estimated by comparison with the intensity of marker bands to make appropriate aliquots.

2.2.3.3 Electroporation of BHK21 cells with RNA

BHK21 cells that were 80-90% confluent were washed once with 10 ml Opti-Mem1, trypsinized and dissociated. The cell suspension was put in a 15 ml Falcon tube with OptiMem1+5% FCS. Then the cells were centrifuged (1300 rpm, 20°C, 3 min) and washed with OptiMem1 three times. After another centrifugation step they were counted in a counting chamber. The cells were again centrifuged (1300 rpm, 20°C, 3 min) and resuspended in an appropriate amount of medium to get 1×10^7 cells/ml. From this suspension 8 μ l per well were seeded in a 6-well plate and incubated (37°C, 5%) for the determination of virus titer the next day. The electroporation was performed with 10 μ g RNA and 10 μ g helper2 RNA in 400 μ l of BHK21 cell suspension in a Gene Pulser cuvette. The zero value was obtained with medium only in the cuvette. The conditions for the Gene Pulser II (Biorad) were adjusted to 360 Volts and 0.075 μ F and the sample was pulsed twice. The content of the cuvette was transferred to prewarmed OptiMem1 with 2.5% FCS in a cell culture flask and incubated at 31°C, 5% CO₂ for 24 hours. During this time the virions are released in the culture medium. Following this incubation, the supernatant was collected and centrifuged to remove debris. Aliquots of 450 μ l supernatant containing virus were snap-frozen in liquid nitrogen and stored at 80°C.

2.2.3.3.1 Virus titer test

The resulting virus has to be activated by the enzymatic activity of a protease. After activation by chymotrypsin, packaged SFV1 particles are fully capable of a single cycle of infection. For virus activation, 450 μ l OptiMem1 with 0.2% BSA was added to 450 μ l virus content and incubated with 100 μ l chymotrypsin for 40 minutes at RT. Then the reaction was stopped by incubation with aprotinin for 10 min. Dilutions of activated virus in medium (0.2% BSA) were made (1:20; 1:200) and, after washing the wells with 3 ml medium, 1ml of the dilutions was added to each well. After 90 minutes incubation (37°C, 5% CO₂) the virus containing supernatant was replaced by OptiMem1 with 2.5% FCS. Cells were incubated on (37°C, 5% CO₂) and the virus titer was calculated.

The virus construct is coupled to m-RFP to determine the number of infected cells by fluorescence. The red cells were counted using an epi-fluorescence microscope (Nikon TS-100F) with a mercury lamp (model name: C-SHG) and a HQ-filter set for enhanced GFP (AHF, Tübingen, Germany).

The titer was calculated with the formula:

number of infected cells x factor for magnification x dilution x dilution factor 2.4

The dilution factor is calculated from the addition of the different solutions, i.e. volume of virus, medium, chymotrypsin and aprotinin divided by virus volume.

2.2.3.4 Infection of bovine chromaffin cells

For overexpression experiments with pSFV1-NPY-mRFP-IRES-Munc13-1-eGFP chromaffin cells were infected with 300 μ l virus solution (prepared as in 2.2.3.2) and incubated for 12-15 hours (37°C, 9%CO₂). The control cells with pSFV1-NPY-mRFP and cells infected with pSFV1-NPY-mRFP-IRES-TeNT-eGFP (100 μ l/well) were incubated for 8-12 hours. These times were chosen so that the cells had approximately the same expression level. The control was taken to see whether the virus construct without protein had any effect on the measurements.

2.2.4 TIRFM

2.2.4.1 Setup

The setup used for the Munc13-1 experiments and the PMA experiments consisted of an inverted Olympus IX 70 microscope, a solid state laser system (85YCA010, Melles Griot, Carlsbad, CA, USA) emitting at 561 nm coupled through a single light guide with a monochromator (Visichrome, Visitron systems GmbH, Puchheim, Germany), a TILL-TIRF condenser (T.I.L.L. Photonics, Gräfeling, Germany) and an Acousto Optical Tunable Filter (AOTF)-nC (AA opto-electronic, St-Rémy-les-Chevreuses, France). The excitation/emission wavelengths were selected with a dual band FITC/Texas red set (# 51006, AHF Analysentechnik AG, Tübingen, Germany). The setup was equipped with a Micromax 512 BFT camera (Princeton Instruments Inc., Trenton, NJ, USA) controlled by Metamorph (Visitron, Puchheim, Germany). A 100x/1.45 NA TIRF oil-immersion objective (Olympus, Hamburg, Germany) was used for the PMA experiments (Pixel size here was 130 nm), while a 60x/1,45 NA TIRF oil-immersion objective (Olympus, Hamburg, Germany) was used along with the 1.5x magnification for the Munc 13-1 experiments (The pixel size was 144 nm).

The setup used for the TeNt experiments consisted of an inverted Zeiss Axiovert 200 microscope (Carl Zeiss, Göttingen, Germany), a 100x/1.45 NA oil-immersion objective (The pixel size was 150 nm) (Carl Zeiss, Göttingen, Germany), a solid state

laser system (85YCA010, Melles Griot, Carlsbad, CA, USA) emitting at 561 nm, a TILL-TIRF condenser (T.I.L.L. Photonics, Gräfeling, Germany). The excitation/emission wavelengths were selected with a dual band filter set (# 20 488020-0000, Carl Zeiss, Göttingen, Germany). The setup was equipped with an Ixon CCD camera (DV 887, Andor Technology LTD, Belfast, Ireland), controlled by a homemade program in LabView.

2.2.4.2 Experimental protocols

A. PMA experiments

Cells were plated as described in section 2.2.1 and incubated for 48 hours to allow good adhesion of the cells on the coverslips. Cells were infected with pSFV1-NPY-mRFP. Cells were recorded for 2 min at rest with 10 Hz acquisition rate in stream mode (which is the mode where the camera can acquire images in the fastest way) and 100 ms exposure time. Then the cells were incubated for 2 min in 250 nM PMA and then washed with Ringer solution for 50 s. Another movie was recorded of the same cell for 2 min followed by a 10 s depolarization with high K^+ solution. Only the cells that exhibited secretion were analyzed.

To test whether TIRFM gives qualitatively similar results to those shown in membrane capacitance recordings, I performed depolarization experiments on cells electroporated with NPY-mRFP that contain a high density of stained vesicles. Cells were recorded for 1 min then depolarized with high K^+ for 20 s then incubated for 2 min in ethanol (control) or in 250 nM PMA. Cells were washed with Ringer's solution for 1 min then depolarized a second time with high K^+ . The number of secreted vesicles at each depolarization was counted.

B. Munc 13-1 experiments

Cells were plated as described in section 2.2.1 and incubated for 48 hours to allow good adhesion of the cells on the coverslips. The control cells were then infected as described in section 2.2.3.4 with pSFV1-NPY-mRFP-IRES-Munc 13-1-eGFP to overexpress Munc13-1 and with pSFV1-NPY-mRFP as control. For both conditions, 3 min movies were acquired in timelapse mode with 5 Hz acquisition rate. The cells were continuously perfused with Ringer's solution. After 2 min of recording, the Ringer's solution was interrupted and high K^+ solution was applied to the cell for 20 s. Secretion was determined as the disappearance of a vesicle in an interval of only

one frame. The count of the number of vesicle per frame was done by a routine in Metamorph after background subtraction.

To verify whether co-expression of NPY and Munc13-1 yielded the same increase in secretion as when Munc13-1 was overexpressed alone we measured the increase in capacitance of cells infected with both viruses after depolarization (NPY-mRFP-IRES-Munc13-1-eGFP and pSFV1-Munc13-1-eGFP previously used by Ashery et al. 2000). The measurements were done using an EPC-9 patch clamp amplifier (HEKA, Lambrecht, Germany). The train of depolarizations consisted of 7 depolarizations from -70 mV to 0 mV with 100 ms duration separated by a 100 ms interval during which a sine wave protocol was applied in order to measure capacitance. The measurements were further analysed in IGOR (WaveMetrics, Portland, USA).

Electrophysiological experiments were performed with the help of U. Becherer.

C. TeNt experimints

Control cells were infected with pSFV1-NPY-mRFP-IRES-TeNt-eGFP to overexpress TeNt and with pSFV1-NPY-mRFP as control. Cells were recorded for 2 min with an acquisition rate of 10 Hz and an exposure time of 90 ms. Cells were continuously perfused with Ringer's solution.

A few cells overexpressing TeNt were tested for secretion using whole cell patch capacitance measurements as described above.

Electrophysiological experiments were performed with the help of M. Pasche.

All experiments were performed at room temperature.

2.2.5 Analysis of movies

The movies acquired were processed using a program developed in house (Dr. Hof) using LabView.

A. Vesicle detection:

Every frame of the stack was first high-pass filtered using a Fast Fourier Transform (FFT), i.e. regions with low spatial frequency are darkened while regions with higher spatial frequencies are left unchanged. Thus, so-called long-scale objects like haze are removed and contrast is enhanced (Fig. 9)

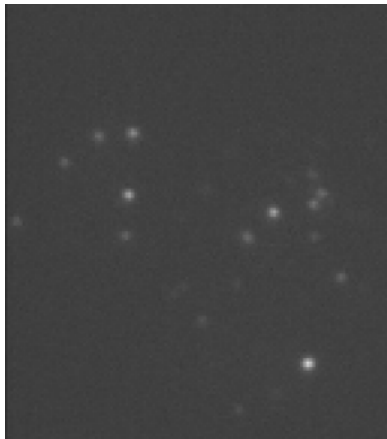


Fig. 9: Frame before FFT-high pass filtering



Frame after FFT-high pass filtering

Then every frame is “thresholded”: Pixels whose grey level lies within a lower and upper limit were assigned the value 1, while all other pixels were assigned the value 0, thus creating a binary frame (Fig. 10). Only those particles whose pixel number is within a defined range (e.g. 3-15 pixels large) are selected as vesicles. The exact position of a vesicle is defined by its centre of mass, while its brightness is determined using the intensity of the original frame.

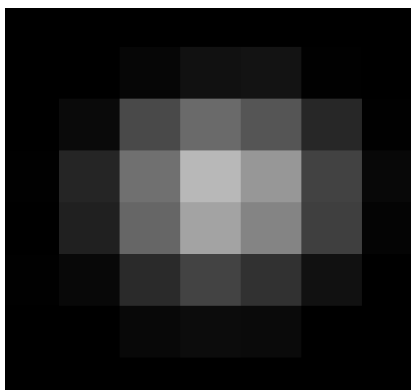
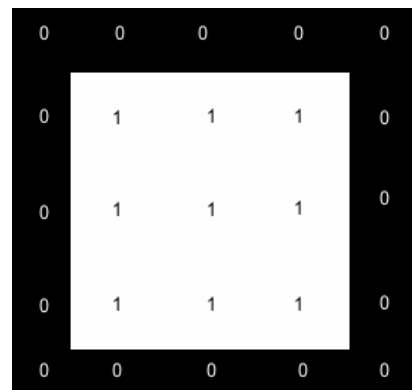


Fig. 10: Actual frame



Binary frame

B. Trajectory determination:

When vesicle detection is completed for all frames of the movie, the tracking algorithm is started. The following procedure is carried out for all frames in the stack, beginning with frame 0 and vesicle 0:

For vesicle n in frame 0, new positions in frame 1 are determined. A radius of 3 pixels is determined; if a vesicle in frame 1 falls within this radius of the position of vesicle n in frame 0, then the vesicle is identified as vesicle n and its position is added to the trajectory (the sum of all positions occupied by the vesicle). If the new position does not fall within the radius of the position in frame 0, the track is terminated e.g. in fig. 11, in the four first frames the positions are in close proximity thus these positions are assigned to only one vesicle. However, the position in the last frame is at a greater distance, thus this position is assigned to another vesicle.

We analyzed trajectories only if vesicles were visible for at least three consecutive frames. When two trajectories overlap and it is no longer possible to distinguish between them, we assign the resulting track to one of the vesicles and the other vesicle is no longer tracked. And of course, trajectories belonging to certain vesicles are no longer available for other vesicles.

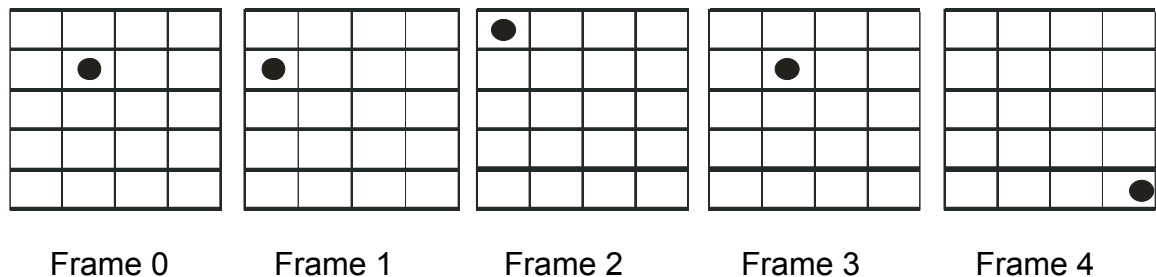


Fig. 11: Tracking of a vesicle.

Sometimes the program loses track of a vesicle for a number of frames due to an intensity decrease below threshold level, resulting in two or more trajectories describing the fate of a single vesicle; yet that the vesicle is still visible by eye. To overcome this problem, a merging routine is provided which merge the two components of this trajectory provided that the track was lost only during a few frames.

A. Resulting files:

In the end of the tracking procedure three files are obtained:

One containing the xy position and the fluorescence of the vesicles vs. time and frame number.

One containing the lateral, axial and 3D velocities of the vesicles.

One containing the MSD vs. Δt values of the vesicles tracks.

2.2.6 Analysis of caging diameter

After obtaining the xy positions of the vesicles, this information was processed in IGOR as follows:

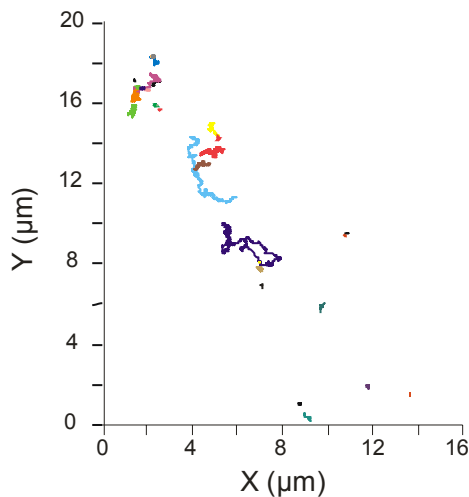


Fig. 12: The xy positions of the vesicles of a single cell were plotted:
Each color represents the trajectory of one vesicle

The caging diameter (CD) is determined: the CD is the maximum distance measured between two positions occupied by the vesicle in a sliding time window of 6 s. The routine starts from the 1st position occupied by a vesicle and measures the distance between this position and all consecutive positions in a window of 6 s. The largest distance measured is taken as CD for this position (Fig. 13). Then the program moves to the 2nd position of the vesicle and repeats the previous steps. This routine is repeated up to the end of the trajectory of the vesicle. Due to the fact that our time window is 6 s, vesicles that are visible for less than 6 s are not taken into consideration in the analysis of the CDs.

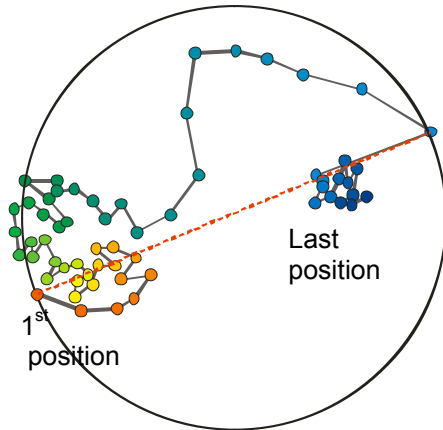


Fig. 13: positions occupied by a vesicle within 6 s starting from the red and ending at the dark blue, red line represents the CD.

When all the CDs are calculated from all the vesicles in a cell they are concatenated in a plot of CD versus time (Fig. 14).

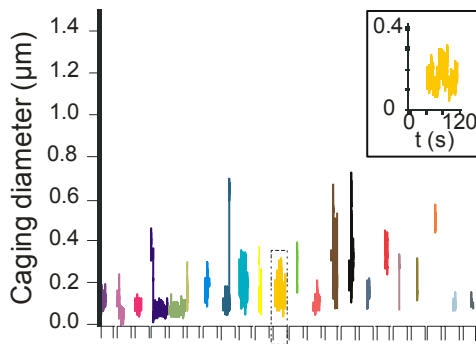


Fig. 14: CD vs. time. Every color represents the CD of one vesicle over time. Inset shows the CD of one vesicle over the 2 min of recording.

A histogram of the CDs is then derived from the previous plot and then a cumulative histogram is plotted (Fig. 15)

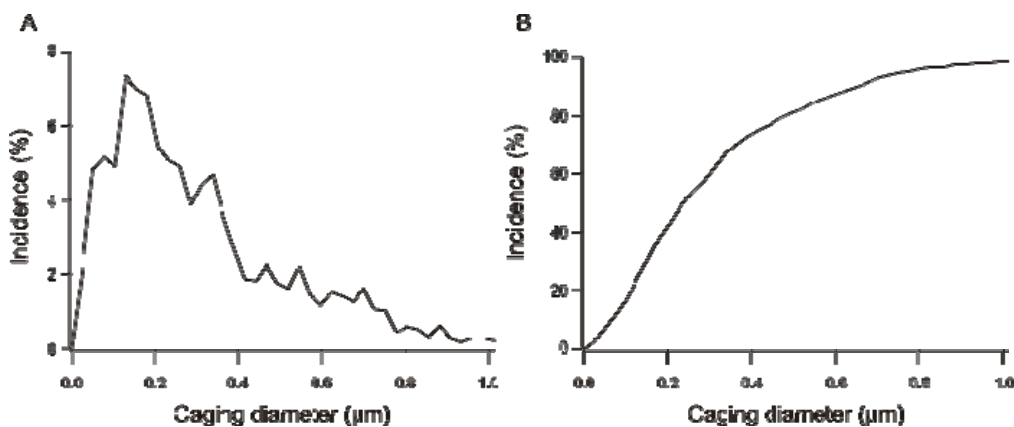


Fig. 15: Size distribution of CD. A, Histogram of CD. B, Cumulative histogram of the CD.

Other parameters are derived from the analysis of the CD and will be discussed in the results.

This method of analysis enables us to actually see the changes of mobility over time, thus it might allow the visualization of the dynamic changes occurring during the lifetime of the vesicle. In contrast, the analysis of the Mean Square Displacement (MSD) (Qian et al. 1991) cannot show the changes in mobility occurring during the lifetime of the vesicle; it only gives an overall description of the mobility of the vesicle as if it had only one type of mobility. In Fig. 16, part of a trajectory of a vesicle is illustrated. The green circles represent the positions occupied by the vesicle starting from light to dark green; the blue line represents the distances taken to calculate the MSD for the first increment which in this example is 100 ms. The red and black lines represent the distances taken to calculate the MSD for the second and third increment respectively.

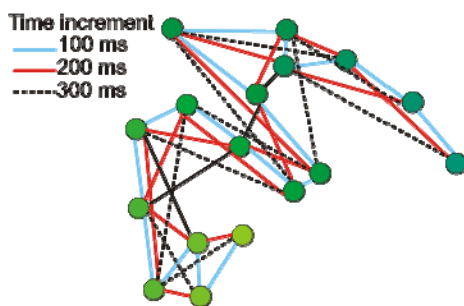


Fig.16: trajectory of a vesicle used to calculate the MSD.

Then the MSD vs. Δt is plotted and the curvature of the MSD gives an indication as to the nature of the motion studied. If the curve saturates (increases then reaches a plateau) then the vesicle is moving within a cage or restricted space. The diffusion coefficient is then derived from the plot and if the coefficient is low then the vesicle is considered immobile otherwise it is considered caged. If the curvature of the MSD plot increases exponentially then the vesicle is considered to have a directed motion. If the curvature is linear, then the vesicle is considered to have a random motion. In some cases, the analysis of the MSD gives an accurate interpretation of the motion of the vesicle but in other cases it does not.

For example, Fig. 17A shows the trajectory of a vesicle that was immobile in the red area then entered a phase where it had a directed motion (green area) then the vesicle was moving in a restricted area (blue area). This is just a very general description.

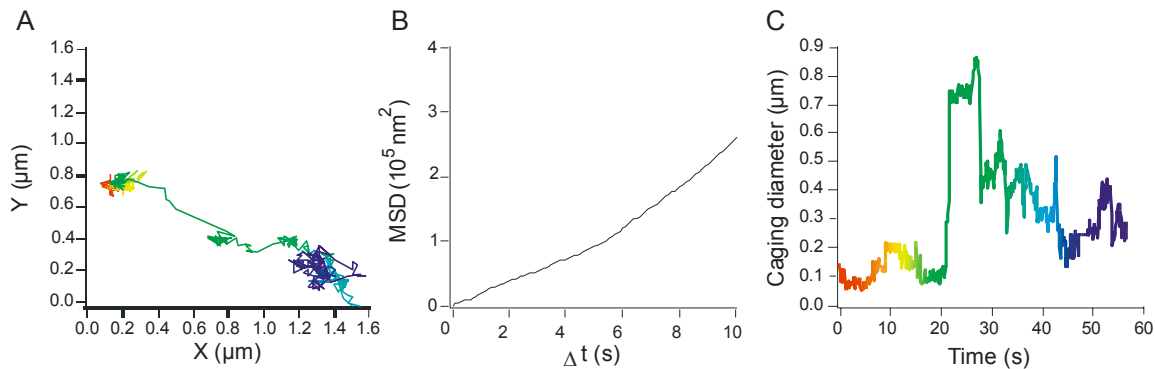


Fig. 17: Comparison between the analysis of the MSD and the CD. A, XY position of an exemplary vesicle. B, MSD vs. Δt of the trajectory of the vesicle. C, CD vs. time of the trajectory of the vesicle.

The MSD of this track was calculated and plotted (Fig. 17B). Since this vesicle shows a multitude of different motions, the expected curvature would be a linear increase with time increment to be interpreted as random walk. But a curve showing an exponential increase with the time increment is obtained, denoting directed motion. This is not the case but the short period of time where the vesicle has a directed motion (green area) dominates the overall motion of the vesicle and this is the reason the MSD gives a false result. The plot of the caging diameter on the contrary shows that the vesicle had a low caging diameter in the beginning of the trajectory (average CD=120 nm) (Fig. 17C). Then the vesicle entered the phase of directed motion and the CD showed a great increase to 0.8 μm . In the end, when the vesicle was moving in a restricted area, the CD was around 342 nm. So the analysis of the CD gives an accurate description of the vesicle's motion over time.

2.2.7 Statistical analysis

Statistical analysis was performed in SigmaStat using Student t-test analysis paired or independent.

For comparison of data that was found to have a skewed distribution, the Mann-Whitney test was used.

For comparison of cumulative distributions, the Kolmogoroff-Smirnoff test was used.

3. Results

3.1 Effect of PMA on bovine chromaffin cells

3.1.1 Effect on secretion

In previous studies (Gillis et al. 1996; Smith et al. 1998), PMA was found to significantly increase secretion as determined using membrane capacitance measurements. We have used PMA to enhance priming and have used TIRFM to detect release of vesicles. This experiment was performed to show that TIRFM gives qualitatively similar results to those observed in membrane capacitance measurements. Bovine chromaffin cells (BCC) were electroporated with NPY-mRFP to obtain a high density of stained vesicles ($1 \text{ vesicle}/\mu\text{m}^2$). Test cells were recorded for 2 min at 10 Hz and then depolarized for 20 s with 90 mM KCl solution to determine a baseline for secretory activity. The cells were then incubated for 2 min in 250 nM PMA; washed for 1 min with Ringer's solution, then depolarized a second time. Control cells were treated similarly except that they were incubated with ethanol (final concentration 3%) instead of PMA as ethanol was the solvent of the PMA solution. The number of vesicles per frame in control and test cells was not different nor was the number of vesicles per frame after PMA treatment different from that before PMA treatment (Fig. 18A). This shows that PMA has no effect on docking as demonstrated previously (Gillis et al. 1996; Smith et al. 1998). Vesicles were considered to be secreted when they disappeared suddenly within one interval (100 ms). The numbers of secreted vesicles was normalized to the number of vesicles per frame prior to the depolarization, so that the fraction of vesicles secreted could be compared. To compare the secretion events, I compared the ratios of the 2nd over the 1st secretion of the PMA treated cells with that of the control cells e.g. if the number of vesicles/frame=10 before depolarization and 11 afterwards, and the number of secretory events at the 1st stimulation is 3 and 2 at the 2nd then the ratio is =2:11/3:10.

The distribution of the secretion events was not bell shaped but skewed to the left, so a non-parametric test was used (Mann-Whitney) to compare the ratios (Fig. 18B).

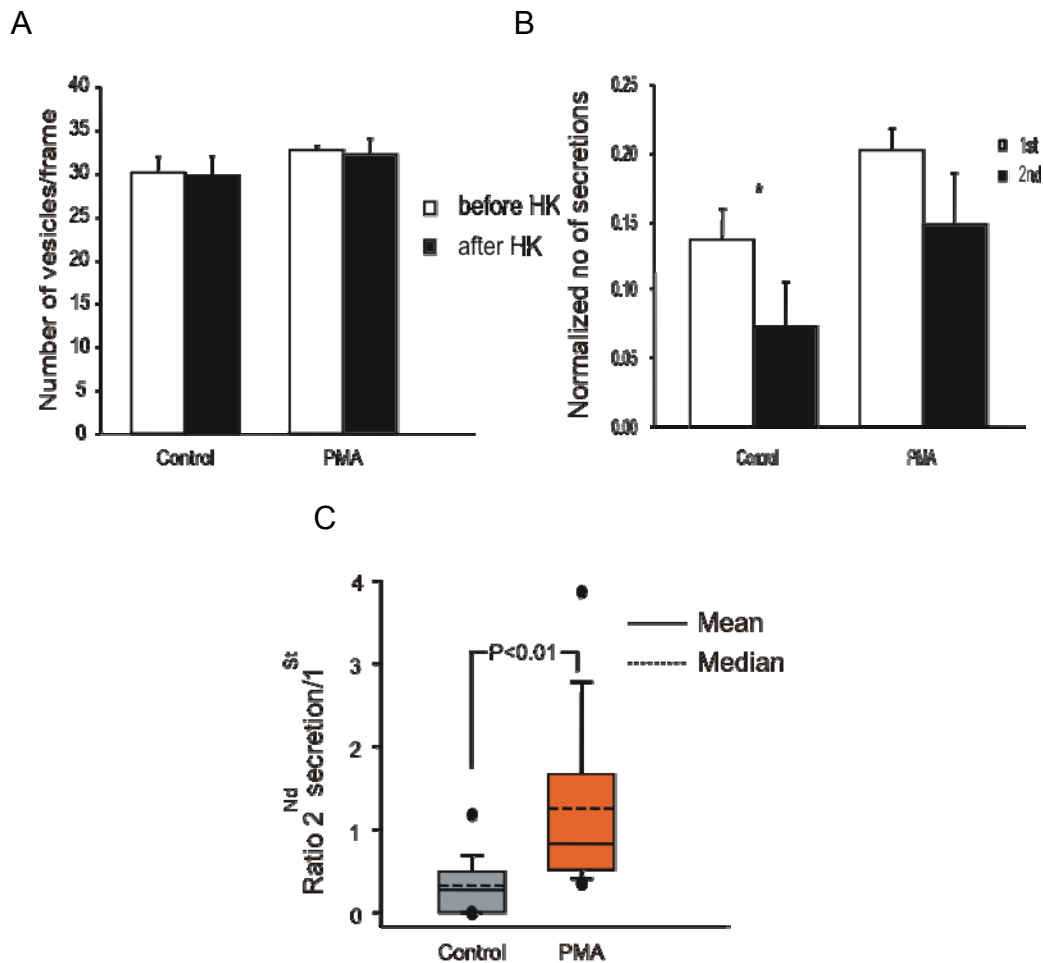


Fig. 18: Effect of PMA on the number of docked and secreted vesicles. A, the number of vesicles/frame before and after HK application was not changed after PMA treatment. B, number of secretions normalised to the number of vesicles/frame before each stimulation. Error bars represent SEM. *, $p < 0.05$. C, the ratios between the second and the first secretion were calculated and the medians were compared using a Mann-whitney test. Secretion was tripled after PMA treatment.

This test compares the medians and not the averages as is the case in normal student T test. In Fig. 18B, the solid line represents the means and the dashed line represents the medians, error bars represent 75% percentiles and the black circles represent values that are outside of the 75% confidence interval. Using this test, secretion after PMA treatment was found to be three times higher than secretion in control cells. Thus, TIRFM gives qualitatively similar results to those obtained using membrane capacitance recordings.

When TIRFM can give us correct information about the fusion step, it could also give us direct information about processes that occur prior to fusion. We propose to monitor the changes in mobility that occur during priming. We expect to be able to show that priming leads to a certain type of motion.

3.1.2 Mobility of vesicles in cells treated with PMA

As PMA specifically promotes priming and as our hypothesis is that priming -which probably corresponds to SNARE complex formation- leads to a reduction in the mobility of LDCVs, I devised the following experimental protocol (Fig. 19) to test this hypothesis. Using this protocol, I could compare the mobility of LDCVs before and after priming with PMA in the same cell. Thus the cell acts as its own control which allows the reduction of variability between cells and also allows us to use paired Student t test.

BCC were infected with pSFV1-NPY-mRFP for 10 hrs before the start of the experiment.

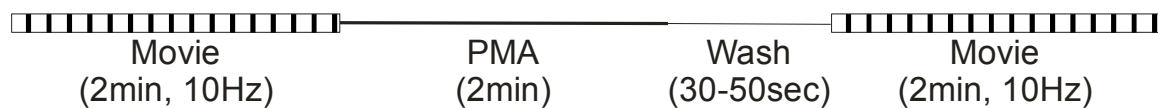


Fig. 19: Experimental protocol

Vesicles were tracked as described in the methods section and the caging diameter was determined. Fig. 20A depicts the trajectories of LDCVs of a representative cell before (control) and after PMA application. It is easily seen that most large range movements of LDCVs disappeared after PMA application. The CD analysis of the LDCVs movement shows that before PMA application most LDCVs moved over a large distance while only few vesicles were immobile (Fig. 20B, right panel). Indeed, many LDCVs had, at least transiently, CDs exceeding 400 nm, which means that within 6 s the LDCVs had a displacement greater than 400 nm. Moreover, only a small fraction of vesicles were immobile since few LDCVs had CDs near 100 nm. After application of PMA, the mobility of LDCVs was dramatically changed (Fig. 20B, left panel). Indeed, many vesicles were nearly immobile displaying CDs of about 100 nm and only few moved over large distances as the CDs of most LDCVs stayed below 400 nm. The histogram of the CDs of this exemplary cell (Fig 20C) shows a large increase in the incidence of CDs having low values after PMA treatment. To illustrate this finding in a simple manner, the normalized cumulative histogram of the CDs of all LDCVs of this exemplary cell is plotted and shows a large leftward shift indicating that vesicles lost mobility after PMA application as compared to control conditions (before PMA application, Fig. 20D). The 50% value of the normalized cumulative histogram revealed a leftward shift of 156 nm for this exemplary cell.

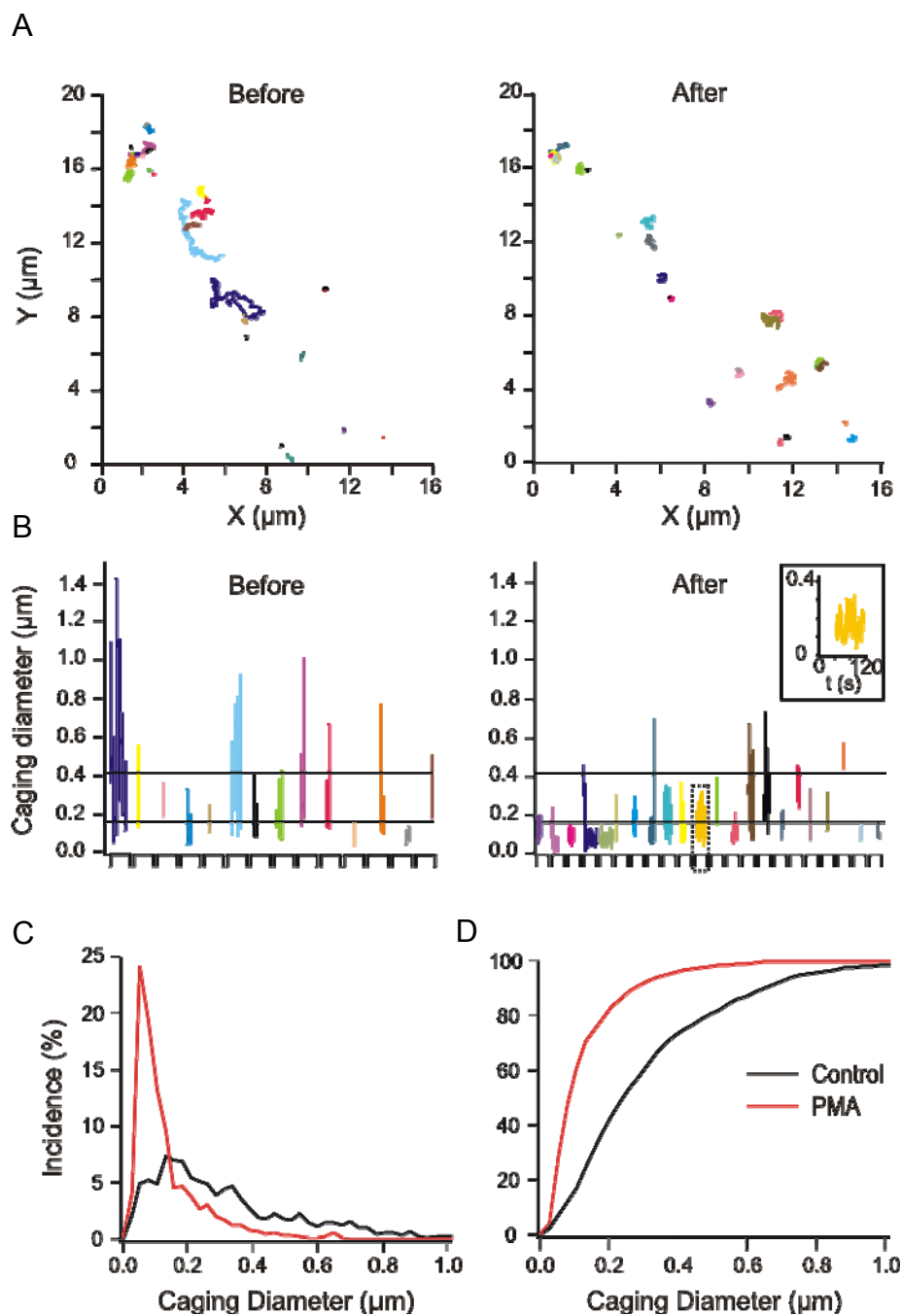


Fig. 20: Analysis of CD in an exemplary cell. A, XY position of the vesicles in the cell before and after PMA treatment, each color represents the trajectory of a vesicle. Note that large tracks such as the dark blue one are rare after PMA treatment. B, CD over time of the vesicles illustrated in A, inset represents the CD of one vesicle over the 2 min recording time. C, histogram of the CD of the cell before (control, black) and after PMA treatment (red), note the higher incidence of CD with lower values after PMA treatment. D, normalised cumulative histogram of CD of the cell before and after PMA treatment, note the large shift to the left after PMA treatment.

Twenty one cells were analyzed the same way and the cumulative histograms of the CDs were plotted. For simplification two plots are represented in Fig. 21A. Note that there was a large variability between cells; some had large left shifts while some had almost none. To obtain a value of the reduction in the CD after PMA treatment an average histogram for the 21 cells was plotted before and after PMA treatment.

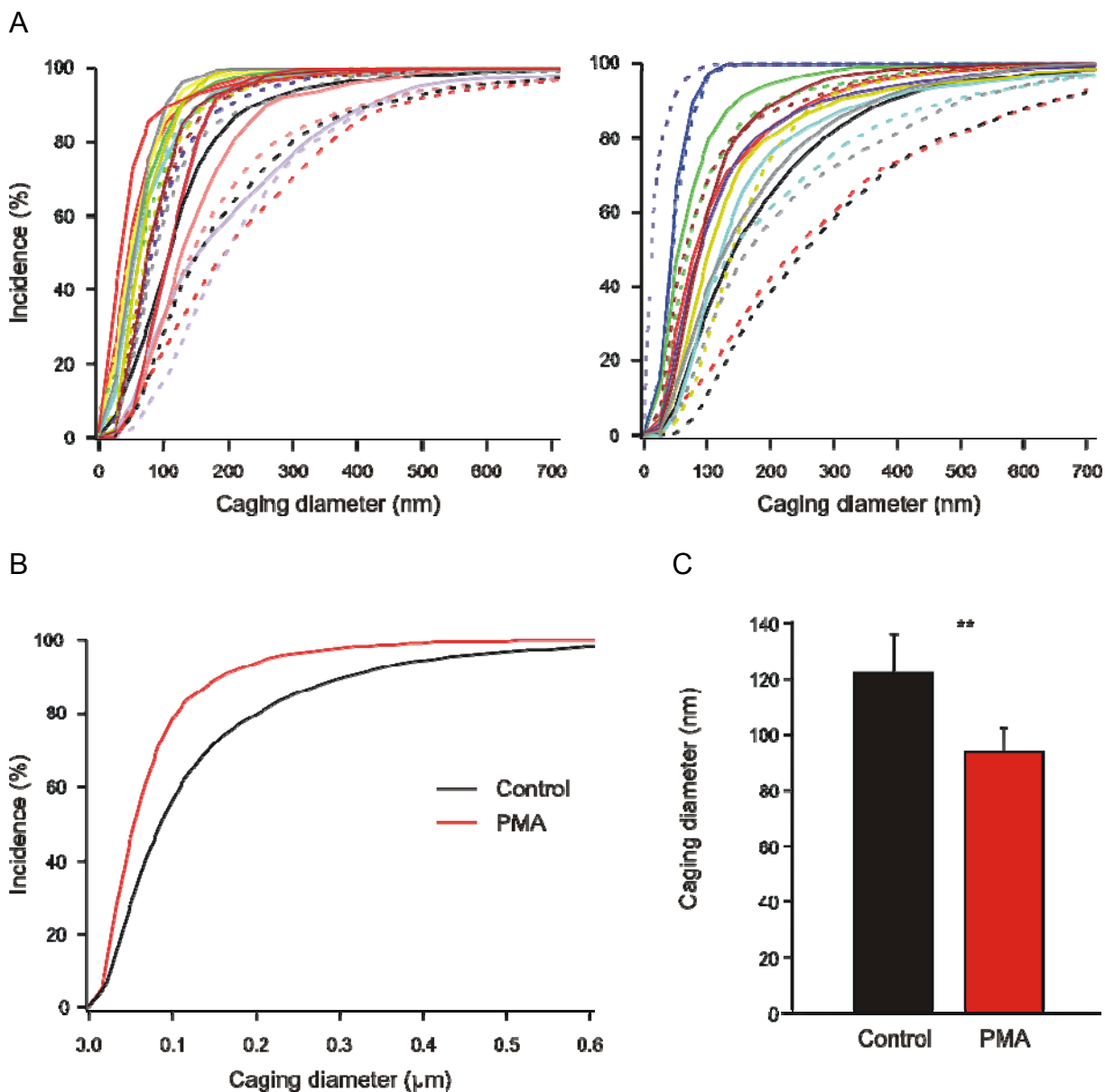


Fig. 21: PMA reduces the mobility of LDCVs. A, normalised cumulative histograms of CDs of vesicles from 21 cells before (dashed lines) and after (solid lines) PMA treatment; each color represents the histogram of one cell. B, normalised cumulative histogram of 21 cells showing a large shift to the left after PMA treatment (N=21, n=417) compared to control (N=21, n=461). C, CD at 50% is significantly reduced after PMA treatment. Error bars represent SEM; **, $p < 0.01$

The cumulative histogram of the caging diameters (Fig. 21B) shows a significant shift to the left after PMA treatment (N=21, n=417) in comparison to those observed in control cells (N=21, n=461). This shift to lower caging diameters after PMA treatment indicates that the mobility of the vesicles is reduced. On analyzing the distributions with the Kolmogoroff-Smirnoff test, the difference was found to be significant ($p=0.05$). The CD after PMA treatment at 50 % of the distribution was also found to be significantly different from that of control (Fig. 20C, $p=0.01$) and the decrease was of 24%.

These results demonstrate that PMA treatment results in a reduction in the mobility of vesicles.

But we could still not distinguish between primed and unprimed vesicles. To do this, we analysed the mobility of secreted vesicles which are primed prior to fusion and the mobility of vesicles that did not fuse with the PM and are not necessarily primed.

3.2 Determination of limits of mobility

Our working hypothesis is that as the SNARE complex is formed during priming and that this complex anchors vesicles tightly to the PM, rendering vesicles immobile. To determine what immobility is in terms of CD, we decided to analyse the mobility of beads (175 nm in diameter) which were fixed on coverslips. We recorded them for 2 min at 10 Hz. The light intensity was adjusted so that their fluorescence intensity was comparable to that of vesicles. After analyzing the CD of the beads, I found that fixed beads had a CD lesser than 100 nm (median=56 nm) (Fig. 22A).

We then analyzed the mobility and the CD of 10 secreted vesicles in the last 15 s of their lifetime. We expected that the distribution of the CD would be similar as that of beads and that the average CD would be comparable with that of fixed beads. However, the histogram of the CD of secreted vesicles had multiple peaks which we have fit using the fit routines of Igor. The individual Gaussian curves are represented as dashed curves in Fig. 22B and C. The first Gaussian had a peak value of 60 nm thus comparable with the median CD of the fixed beads, so we considered this to be jitter inherent in the experimental setup. This peak accounted for 25% of the CDs. The second Gaussian had a peak value of 101 nm and accounted for 58% of the CDs, the third Gaussian had a peak value of 220 nm and accounted for 10% of the CDs while the fourth Gaussian had a peak value of 520 nm and accounted for 7% of

the CDs. Since this distribution included only secreted vesicles, they must have been primed. Since the first peak appears to be experimental jitter, it is likely that primed vesicles belong to the remaining population with the lowest mobility. This is the second peak which is also the most prominent peak (Fig. 22B). The last 2 Gaussians could represent short periods of time where the vesicles unprimed prior to fusion.

To strengthen this conclusion, we analyzed the movement of vesicles that were not secreted ($n=15$), thus were less likely to have been primed (Fig. 22C). The distribution of the CDs could also be fit with 4 Gaussians with the same peak values as those obtained for the secreted vesicles. The first and fourth Gaussians accounted for 30% and 6% of the CD distribution respectively which is similar to the values obtained for the secreted vesicles. As the first Gaussian represents the inherent movement of our recording system, it affects all vesicles equally. The fourth Gaussian represents vesicles with very large movements possibly having a directed type of motion. The integral values of the second and third peaks were different. The integral of the second Gaussian was decreased from 58% to 19%, a third of the value for secreted vesicles. The third Gaussian's integral value was increased by a factor of 4.5 from 10% to 45% as compared to secreted vesicles. Since the vesicles in Fig. 21B were primed and the vesicles in Fig. 22C were docked but not necessarily primed, we deduced that primed vesicles are represented by the second Gaussian having a peak at $CD=101$ nm and that docked but unprimed vesicles are represented by the third Gaussian and have a peak at $CD=220$ nm. So we conclude that primed vesicles were nearly immobile, docked vesicles were caged vesicles or vesicles having a restricted motion and vesicles in the depot pool were vesicles having a directed motion. Since PMA increases the primed pool and decreases mobility, we have tested whether PMA increases the incidence of vesicles exhibiting a CD near 101 nm while reducing that with higher mobilities.

To distinguish nearly immobile from caged vesicles, we used the intersection point between the second and third Gaussian (170 nm, Fig. 22B) and to distinguish caged vesicles from vesicles with directed motion, we used the intersection point between the third and the fourth Gaussian (403 nm).

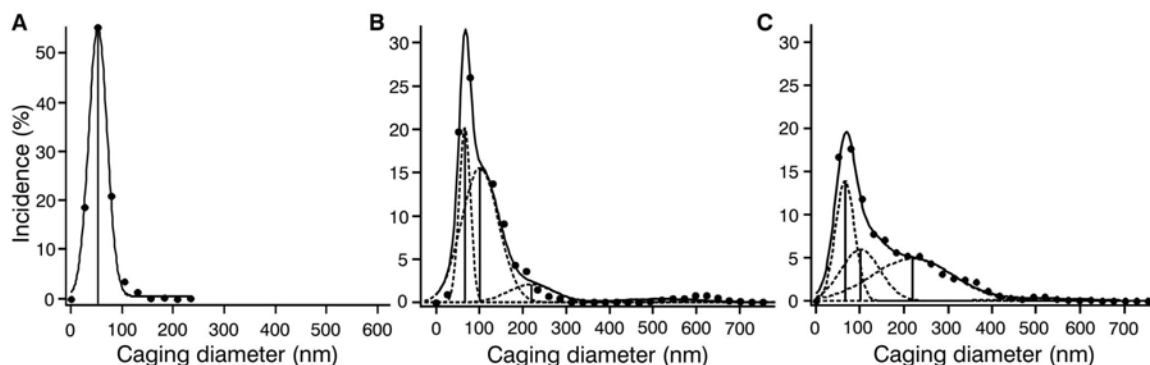


Fig. 22: Size distribution of CD of beads, secreted, and non-secreted vesicles. A, Histogram of CD of beads with a peak value of 56 nm. B, Histogram of CD of secreted vesicles ($n=10$) with peak values and integral values of 60 (25%), 101 (58%), 220 (10%) and 520 nm (7%). C, Histogram of CD of non secreted vesicles ($n=15$) with peak values similar to those in B and integral values of 30%, 19%, 45% and 6%.

As can be seen in Fig. 22B and C, vesicle mobility is not a constant, but can rather change over time. This is to be expected since the transition from the docked state to the primed state is reversible. Therefore, we have followed mobility (CD) over time to determine how vesicle mobility changes. We have, based on these results, defined different types of mobility.

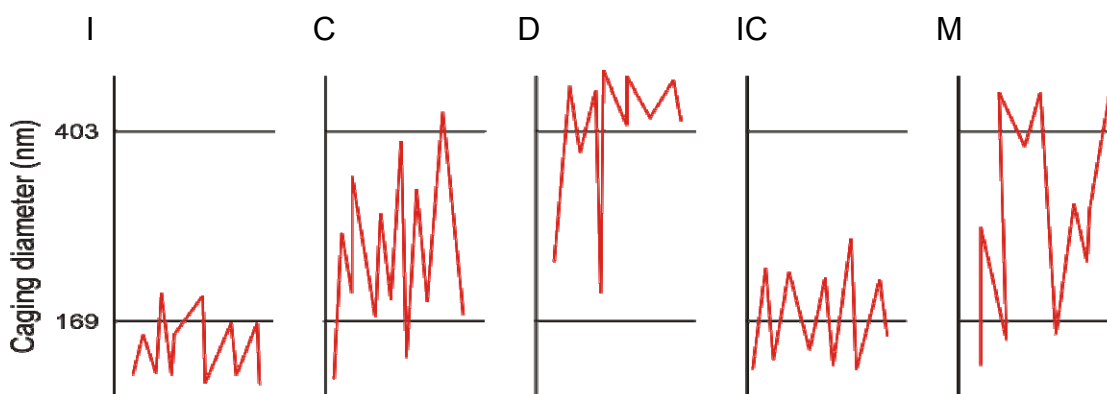


Fig. 23: Classification of vesicles. I, Immobile vesicle: $CD < 169$ nm for 75% of the time. C, Caged vesicle: $169 \text{ nm} < CD < 403$ nm for 75% of the time. D, Vesicle with directed motion: $CD > 403$ nm for 75% of the time. IC, Immobile-caged vesicle: CD oscillating between the I and the C states. M, Vesicle with mixed motion: CD constantly oscillating between the three states.

We considered vesicles as nearly immobile (I) when their CD was below 170 nm for 75% of the time. Vesicles were considered caged (C) when their CD was between

170 nm and 403 nm for 75% of the time. Vesicles had a directed motion (D) when their CD was larger than 403 nm for 75% of the time. Immobile-caged vesicles (IC) were those that spent 75% of the time below 403 nm but whose CD was oscillating between the nearly immobile state and the caged state. Finally, vesicles were considered to have a mixed motion (M) when their CD was constantly oscillating between the three mobility states (Fig. 23).

3.2.1 PMA treatment increases the number of nearly immobile vesicles

I used the previously determined limits to classify vesicles from cells treated with PMA. I expected to observe an increase in the fraction of nearly immobile vesicles after PMA treatment.

The LDCVs of the cells treated with PMA were tracked at rest (before depolarization with the high K^+ solution). The CDs were analyzed and the vesicles classified using the limits determined in the previous section.

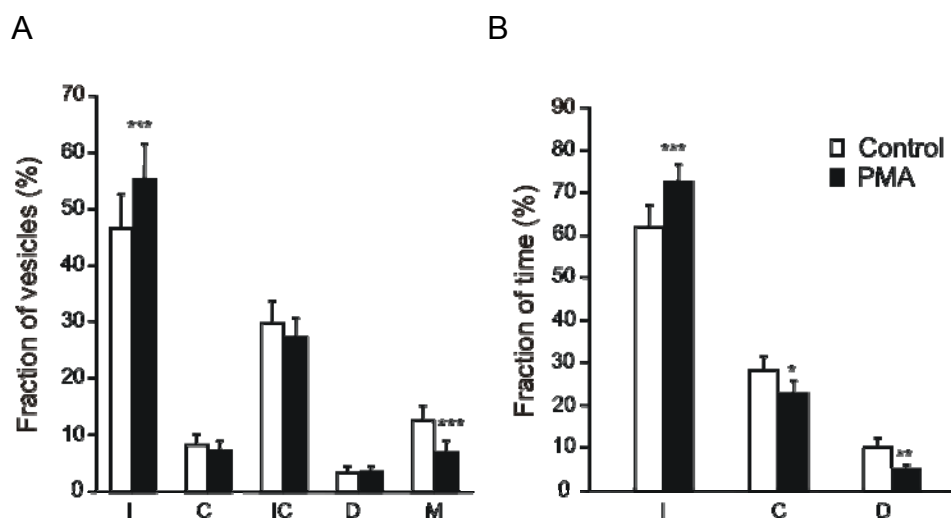


Fig. 24: A, Fraction of vesicles in each type of motion, I=immobile, C=caged, IC=immobile-caged, D=directed motion, M=mixed. The fraction of nearly immobile vesicles significantly increased while the fraction of vesicles with mixed motion was reduced. B, Fraction of time spent in each type of motion. The fraction of time spent in the nearly immobile state was significantly increased and the fraction of time spent in the restricted and directed state was significantly reduced. Error bars represent SEM; *, $p < 0.05$; **, $p < 0.01$; ***, $p < 0.005$; paired student test.

After treatment with 250 nM PMA, the fraction of immobile vesicles increased significantly (N=21, n=417) by 19% ($p=0.0049$) as compared to control cells (N=21, n=461, Fig. 24A). As mentioned before, since priming is believed to be the association of vesicles into SNARE complexes, we hypothesize that priming should lead to immobilization of vesicles.

This result confirms our prediction that priming leads to immobility. This supports the idea that primed vesicles are represented by immobile vesicles. In addition, the fraction of vesicles with mixed behavior was significantly decreased by 45% ($p=0.002$) indicating that when priming was promoted, the mobility of the vesicles was more targeted to definite types of motion (Fig 24A).

Note that the advantage of this experiment was the fact that the cell acted as its own control, thus paired student t-test was used for the statistical analysis and although the SEM bars was large, the changes were still significant.

The fraction of time spent in each type of motion corresponded well with the changes in the numbers of vesicles displaying the different types of mobility. The fraction of time spent in the immobile state was significantly increased (N=21, n=461, $p=0.002$) and vesicles spent significantly less time in the caged state (N=21, n=461, $p=0.016$) and in directed motion (N=21, n=461, $p=0.007$) (Fig. 24B). This indicates that tracked vesicles spend more time in the immobile than in the caged state.

As stated in the methods, our tracking protocol enables us to obtain information on the velocities of the vesicles and their dwell time (the time they remain visible). Table 1 lists the parameters of the tracked vesicles.

The number of tracked vesicles and the number of vesicles per frame were unchanged after PMA treatment indicating that PMA has no effect on docking. Also no effect was observed on the velocity indicating that the increase of the fraction of immobile vesicles was not a result of a reduced velocity. The dwell time of the vesicles was not altered after PMA treatment. Visitors are the vesicles that were tracked but were visible for less than 6 s, thus their CD was not analyzed.

Table 1: Characteristics of tracked vesicles:

	Control	PMA
Number of tracked vesicles	947	848
Vesicles/cell	45.1 ± 5.5	40.4 ± 5.2
Vesicles/frame	11.5 ± 1.0	11.4 ± 1.0
Dwell time (s)	23.1 ± 1.8	27.6 ± 3.4
Average velocity (nm.s ⁻¹)	331.0 ± 20.0	340.2 ± 23.9
Number of visitors	486	431
Visitors/cell	20.0 ± 3.0	20.0 ± 3.7

N = 21, n = 1795.

3.3 Overexpression of Munc13-1 alone and fused with NPY-mRFP.

To check our hypothesis with an independent method, I promoted priming by overexpressing Munc13-1 in BCCs. In previous studies using overexpression of Munc13-1, the protein was fused with eGFP in a pSFV1 plasmid (Ashery et al. 2000). Here I use pSFV1-NPY-mRFP-IRES-Munc13-1-eGFP. To determine whether overexpression of Munc13-1 using this expression vector gives comparable results to those reported by Ashery et al. (2000), I compared the effect of overexpression of Munc13-1 in BCCs. The secretion in overexpressing cells was compared to that in wild type control cells. Cells were measured in the whole cell configuration at room temperature.

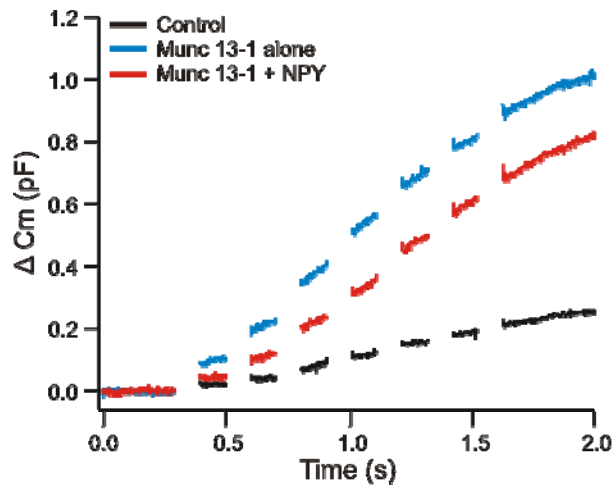


Fig. 25: Expression of Munc13-1 alone and co-expression of NPY and Munc13-1. The black trace represents secretion from control cells after a train of depolarizations. The blue trace represents secretion from Munc13-1 overexpressing cells; secretion was tripled compared to control cells. The red trace represents secretion from cells co-expressing Munc13-1 and NPY. There was no difference between the red and blue traces. Control, n=8; Munc13-1, n=10; Munc13-1+NPY, n=6.

Co-expression of NPY and Munc13-1 yielded a strong increase in capacitance (843.0 ± 221.8 fF, n=6) in comparison to control cells (252.7 ± 57.4 fF, n=8) (Fig. 25). Expression of Munc13-1 alone resulted in an increase in capacitance that is comparable with that of the co-expression of NPY and Munc13-1 (1041.0 ± 239.8 fF, n=10). This shows that the pSFV1-NPY-mRFP-IRES-Munc13-1-eGFP virus is effective in enhancing secretion and thus suitable as a tool to enhance priming. So I used BCC overexpressing Munc13-1 to monitor exocytosis and mobility of vesicles from these cells.

3.4 Effect of Munc13-1 on secretion from chromaffin cells

3.4.1 Munc13-1 increases secretory events observed in TIRFM

The present experiment was performed to confirm that secretion observed using TIRFM is similar to that recorded using membrane capacitance measurements.

BCC were infected with the pSFV1-NPY-mRFP virus for control and with the pSFV1-NPY-mRFP-IRES-Munc13-1-eGFP virus for 12-15 hrs, then a movie was recorded of the cells at rest for 2 min with a frequency of 5 Hz. The cells were then depolarized for 20 s with a high K^+ solution. The total number of vesicles and the number of vesicles per frame were determined using Metamorph. The total number of vesicles and the number of vesicles per frame were similar in control and test cells indicating that Munc13-1 has no effect on docking as stated before (Ashery et al. 2000) (Fig. 26A and B, Table 2).

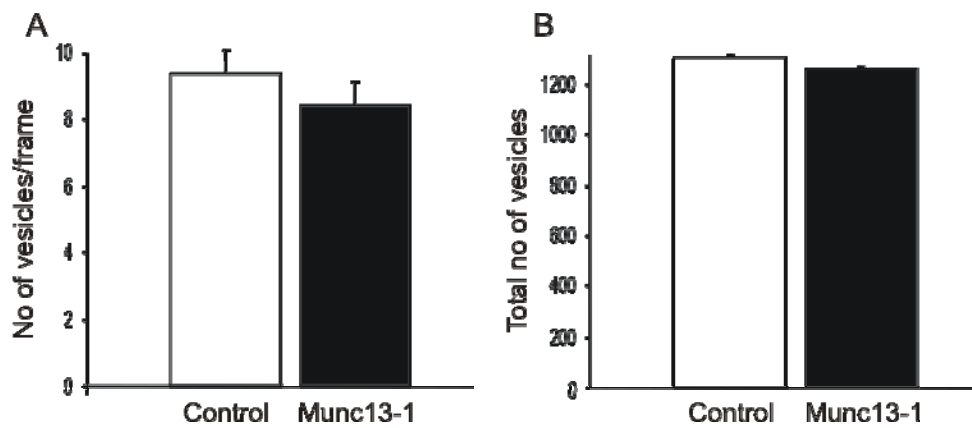


Fig. 26: Munc13-1 has no effect on docking. A, number of vesicles/frame; the number of visible vesicles per frame was similar in Munc13-1 overexpressing cells and in control ones. B, total number of vesicles; the total number of vesicles was similar in Munc13-1 overexpressing cells and in control ones. Control (n=28), Munc13-1 (n=33). Error bars represent SEM.

When a vesicle was visible in one frame then disappeared in the next frame, this was considered a secretory event (after 200 ms). The number of secretory events was then normalized to the number of vesicles per frame. Secretory events were counted over the period of the 20 s of stimulation. The number of secretions was increased by 32% but the difference was not significant (Fig. 27A).

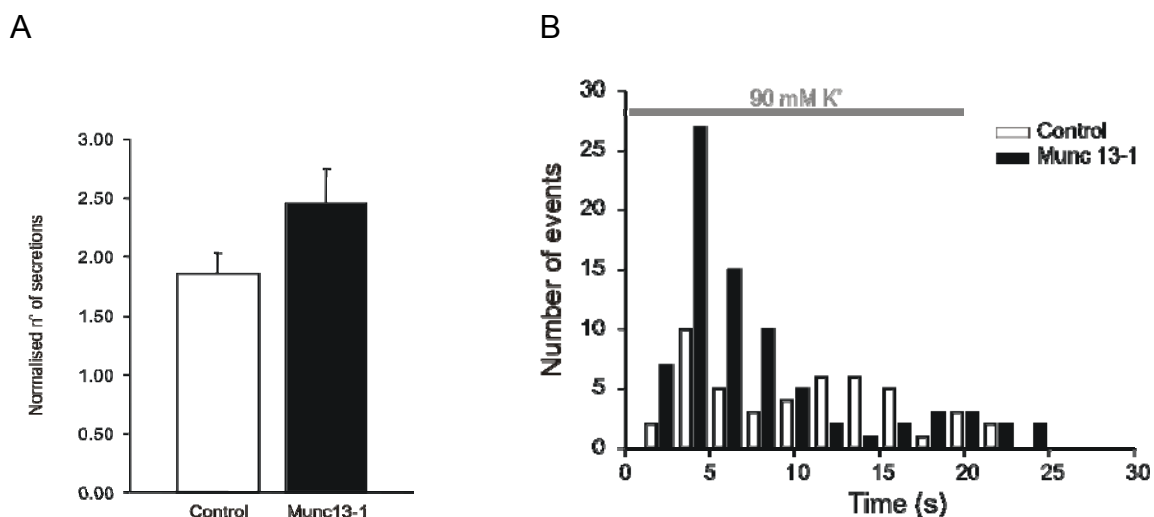


Fig. 27: Secretion in Munc13-1 overexpressing cells. A, Number of secretions normalized to the number of vesicles/frame; Control, n=28; Munc13-1, n=33. The number of secretions in Munc13-1 overexpressing cells increased but was not significant compared to control cells due to the large variability between cells and the long duration of the stimulation protocol (20 s). B, Distribution of secretion over time, bin=2 s. The distribution of secretion from Munc13-1 overexpressing cells shows a peak at 5 s then a gradual decrease (black bars), while the distribution of secretion in control cells is continuous over the time of stimulation (white bars). Error bars represent SEM.

Ashery et al. (2000) have reported an approximately three fold increase in secretion. We observe a similar effect of Munc13-1 overexpression on depolarization induced secretion (Fig. 25). Thus, our results with potassium stimulation indicates a weaker than expected effect of Munc13-1 on secretion observed in TIRFM. This may be due to the relatively long duration of the potassium stimulation. We have examined the time course of secretion in the experiment described in Fig. 27A and found that a strong enhancement of secretion was present in Munc13-1 overexpressing cells in the first 10 s of stimulation (Fig. 27B). This probably shows that the vesicles that are released first are already primed, which also shows that Munc13-1 increases the primed pool as already shown in previous studies (Ashery et al. 2000). So I determined the normalized number of secretory events in the first 10 s of secretion only (Fig. 28). The secretion was tripled in Munc13-1 overexpressing cells ($n=33$) ($p<0.005$) in comparison to control cells ($n=28$). Note that the numbers of secreted vesicles are low because some cells did not secrete in the first 10 s of depolarization thus they were given a value of zero and taken into account in the calculation; also, in virus infected cells, the density of stained vesicles is low ($0.1 \text{ vesicle}/\mu\text{m}^2$) and we obtain cells that secrete only one vesicle per depolarization. From these data, I conclude that Munc13-1 specifically promotes priming since docking was unaffected. We also confirm that TIRFM gives similar results to those obtained by membrane capacitance recordings.

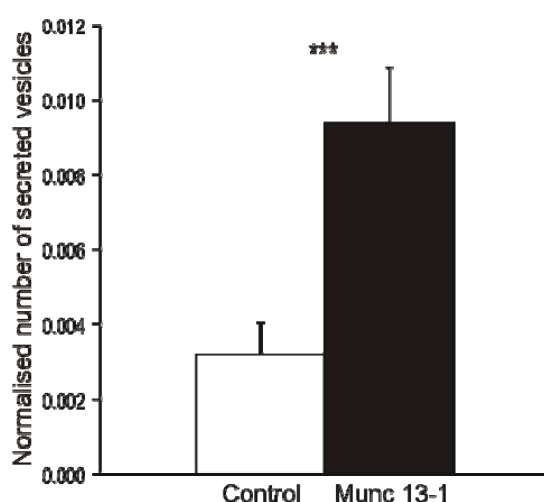


Fig. 28: Secretion in the first 10 s of depolarization. Munc13-1 overexpression triples the number of exocytosed vesicles in the 1st 10 s of depolarization compared to control. Control, $n=28$; Munc13-1, $n=33$. Error bars represent SEM; ***, $p<0.005$.

3.4.2 Munc13-1 overexpression increases the number of immobile vesicles

Since Munc13-1 specifically promotes priming, I decided to test whether overexpression of Munc13-1 has similar effects on mobility as PMA treatment. The cells used in the previous section were used, their LDCVs tracked at rest, and the CDs were analyzed.

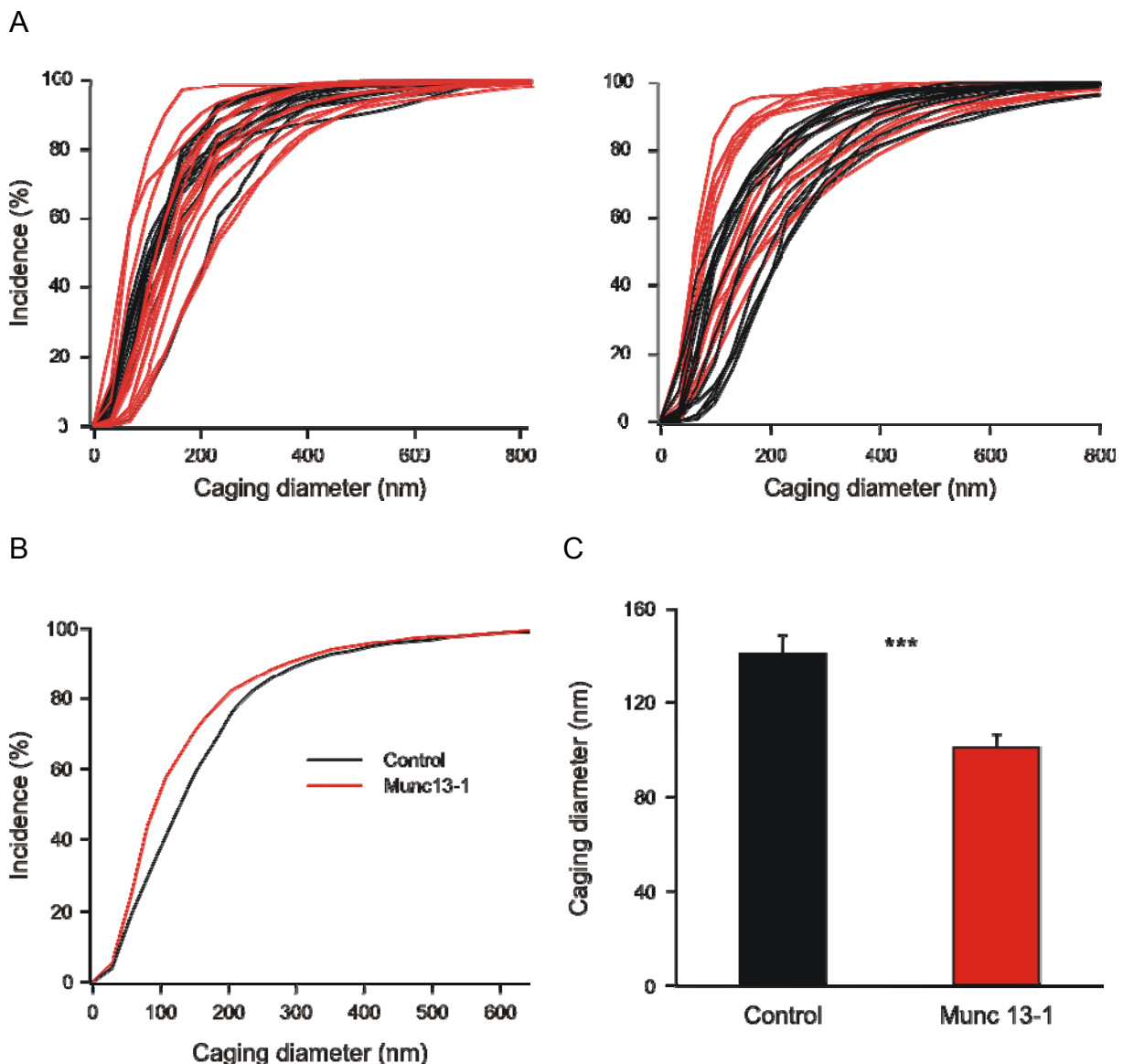


Fig. 29: Munc13-1 overexpression reduces the mobility of vesicles. A, normalised cumulative histograms of 24 control cells (black) and 31 Munc13-1 overexpressing cells (red). B, CD histogram shows a shift to the left in Munc13-1 overexpressing cells; Control N=24, n=686; Munc13-1 N=31, n=695. The difference between the two distributions is significant. C, Shift of the CD at 50%; the decrease is of 40 nm. Error bars represent SEM; ***, $p < 0.005$.

The cumulative histograms of 24 control cells and 31 Munc13-1 overexpressing cells were plotted (Fig. 29A, right and left). These cells cannot be compared in a paired manner like the PMA treated cells were. It is even more complicated to obtain information from such plots. Therefore, the average cumulative histograms of Munc13-1 overexpressing cells and control ones were plotted (Fig. 29B). The cumulative histogram of the CD of vesicles from Munc13-1 overexpressing cells was shifted to the left as was the case with PMA treated cells (Fig. 29B), so the CD was smaller in Munc13-1 overexpressing cells (N=31, n=695) in comparison to control cells (N=24, n=686).

The difference between the two distributions was found to be significant ($p=0.05$, Kolmogoroff-Smirnoff test. Fig. 29B) and the decrease of CD at 50% was of 40 nm and was significant compared to control ($p=0.0001$) (Fig. 29C).

Then the vesicles were classified according to their mobility. In spite of the variability between cells, the fraction of nearly immobile vesicles was significantly increased (68%, $p=0.006$) in Munc13-1 overexpressing cells as compared to control cells (Fig. 30A). On the other hand, the number of caged vesicles was significantly reduced by 46.8% ($p=0.001$), while the number of immobile-caged vesicles did not change. Notably, the number of docked vesicles (sum of nearly immobile, caged and immobile-caged vesicles) was not significantly changed after Munc13-1 overexpression (control, $84.1\pm 6\%$; Munc13-1, $89.6\pm 10\%$) indicating that Munc13-1 has no effect on docking as shown in previous studies. The number of vesicles having directed motion and mixed behavior did not change.

The time the vesicles spend in the immobile state was significantly increased by 33% ($p=0.0002$) in Munc13-1 overexpressing cells compared to control cells (Fig. 30B). The time the vesicles spend in the caged state was significantly reduced by 37% ($p=0.0002$). The time they spend in directed motion was significantly reduced by 43% ($p=0.005$) but these vesicles represent less than 5% of the vesicles in both control and Munc13-1 overexpressing cells.

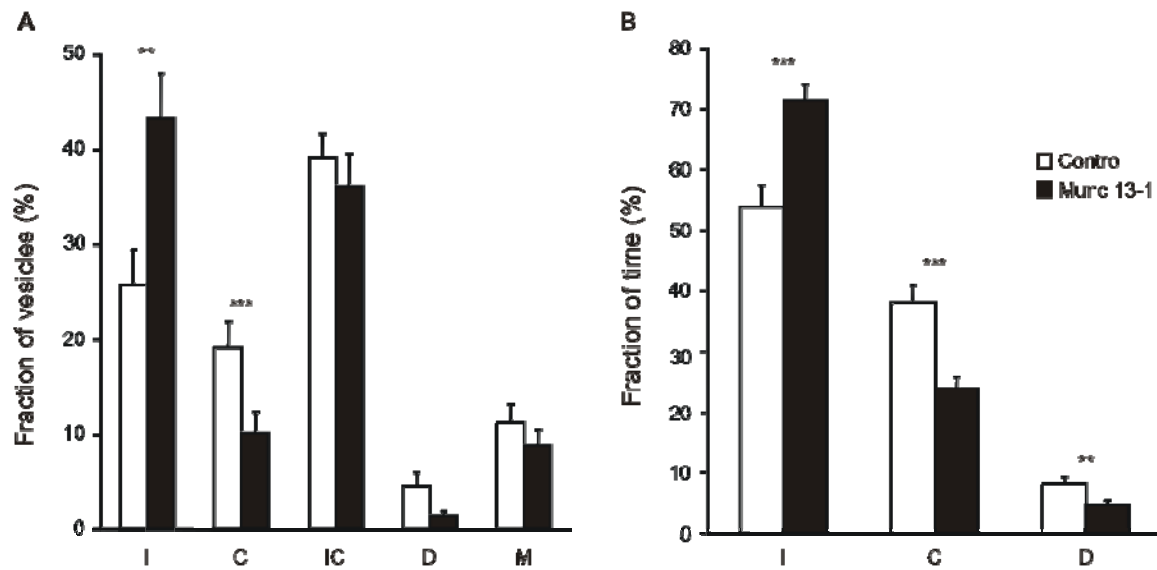


Fig. 30: Munc13-1 overexpression increases the number of nearly immobile vesicles. A, fraction of vesicles in each type of motion. The fraction of nearly immobile vesicles was significantly increased while that of caged vesicles was significantly reduced. B, Fraction of time spent in each type of motion; Control, N=24, n=686; Munc13-1, N=31, n=695. The fraction of time spent in the immobile state was significantly increased while the fraction of time spent in the two remaining state was significantly reduced. Error bars represent SEM; **, $p < 0.01$; ***, $p < 0.005$.

Table 2: Parameters of LDCVs in Munc13-1 overexpressing cells:

	Control	Munc13-1
Number of tracked vesicles	1313	1267
Vesicles/cell	54.7 ± 6.2	36.5 ± 4.9
Vesicles/frame	9.4 ± 1.0	8.7 ± 1.0
Dwell time (s)	22.5 ± 1.7	17.8 ± 2.0
Average velocity ($\text{nm} \cdot \text{s}^{-1}$)	318.8 ± 31.6	256.6 ± 25.5
Number of visitors	627	572
Visitors/cell	26.1 ± 3.7	20.1 ± 2.8

Control: N = 24, n = 1313; Munc13-1: N = 31, n = 1267.

As was the case in PMA treated cells, the parameters of tracked vesicles were unchanged in Munc13-1 overexpressing cells as listed in table 2.

Our previous results obtained from PMA treated cells and the present results from Munc13-1 overexpressing cells show that enhancing priming leads to immobilization of vesicles. This has reinforced our hypothesis that when the vesicles undergo priming when the SNARE complex probably forms, the vesicle becomes attached to the PM and is then not able to move freely.

To challenge our hypothesis, we verified our results by preventing priming. We thus expect to see an opposite effect on mobility to that observed when priming was promoted.

3.5 Overexpression of tetanus toxin light chain increases the mobility of vesicles

To verify our previous conclusions, I have blocked SNARE complex formation which should prevent priming and result in increased mobility of vesicles. I used a virus containing both NPY-mRFP to visualize the vesicles and eGFP-TeNt-LC (the light chain of tetanus toxin) which cleaves synaptobrevin and prevents it from forming SNARE complexes.

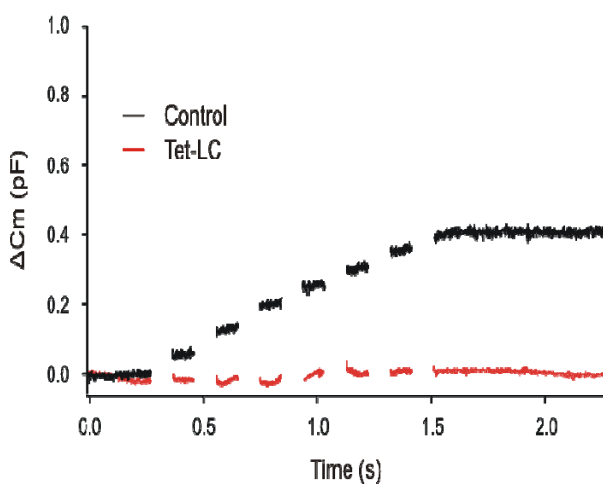
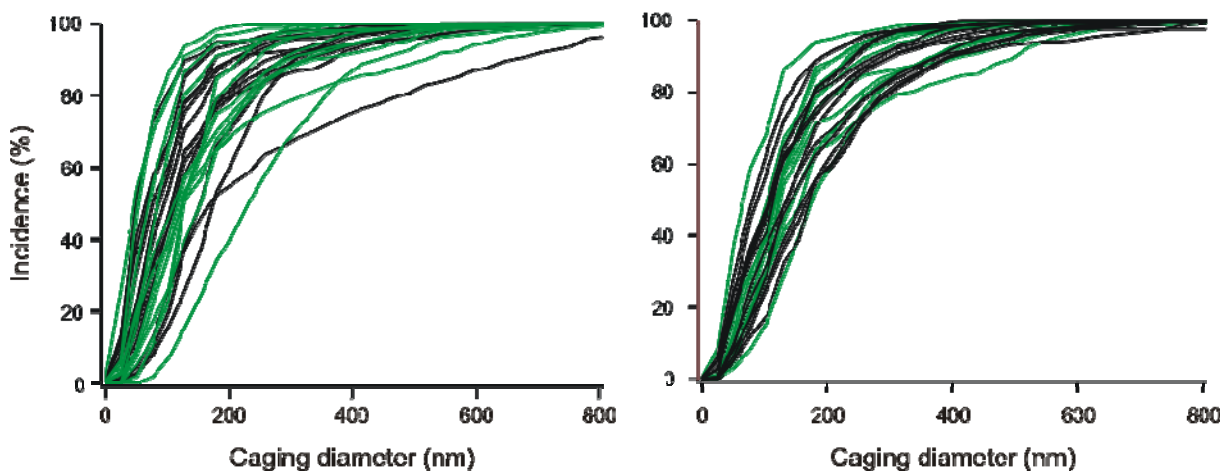


Fig. 31: Secretion in TeNt-LC overexpressing cells: TeNt-LC overexpressing cells (n=4) show a complete block of exocytosis compared to control cells (n=6).

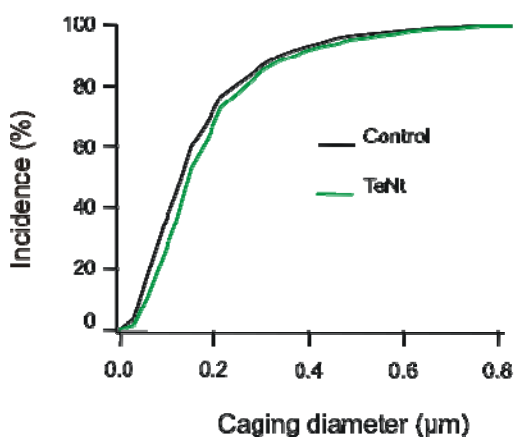
BCC were infected with pSFV1-NPY-mRFP for control cells and with pSFV1-NPY-mRFP-IRES-TeNt-LC-eGFP for 10-12 hrs. To demonstrate that the virus containing the TeNt-LC blocks exocytosis, I performed membrane capacitance recordings on control cells and cells expressing tetanus toxin. Cells expressing TeNt-LC showed a complete block of exocytosis in comparison to control cells (Fig. 31).

Vesicles from control cells and from cells overexpressing TeNt-LC were tracked and their CDs was analyzed. The cumulative histograms of the CDs of 22 TeNt-LC expressing cells and 25 control ones were represented in two plots for clarity (Fig. 32 A). It was impossible to obtain a definit information from these plots.

A



B



C

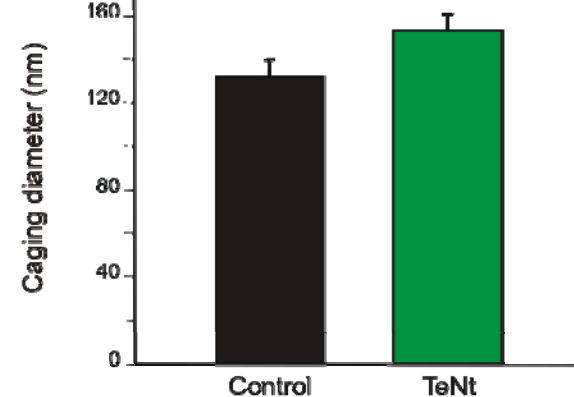


Fig. 32: Overexpression of TeNt-LC increases the mobility of vesicles. A, normalised cumulative histograms of 22 TeNt-LC expressing cells (green) and 25 control cells (black). B, Cumulative histogram of CDs showing a shift to the right in TeNt-LC overexpressing cells (N=22, n=453) compared to control cells (N=25, n=553). C, Shift of CD at 50% showing a significant increase in TeNt overexpressing cells. Error bars represent SEM; *, $p < 0.05$.

Thus, the average cumulative histograms of the CD of TeNt-LC expressing cells and control ones were plotted (Fig. 32B). As expected, the cumulative histogram of the CD of TeNt-LC expressing cells (N=22, n=453) was shifted to the right indicating that the CD was larger so the vesicles have larger movements in comparison to control cells (N=25, n=553) (Fig. 32B).

The reduction of CD at 50% was of 21.5 nm but the difference between the two distributions (control and TeNt-LC expressing cells) was significant ($p=0.03$) (Fig. 32C).

Table 3: Parameters of LDCVs in TeNt-LC overexpressing cells:

	Control	TeNt
Number of tracked vesicles	1213	1267
Vesicles/cell	52.5 ± 4.3	58.5 ± 7.0
Vesicles/frame	6.5 ± 0.5	8.4 ± 0.9
Dwell time (s)	17.0 ± 1.0	$12.6 \pm 0.9^{**}$
Average velocity ($\text{nm}\cdot\text{s}^{-1}$)	532.0 ± 27.0	546.7 ± 31.0
Number of visitors	660	883
Visitors/cell	28.4 ± 2.9	37.9 ± 5.0

Control: N = 25, n = 1213; TeNt: N = 22, n = 1267.

Table 3 shows the parameters of LDCVs of TeNt-LC overexpressing cells compared to control cells. In all previous cases, the fraction of visitors ranged from 50% to 55%, but in TeNt-LC overexpressing cells the fraction of visitors was $63\pm 3\%$ in comparison to control ($55\pm 2\%$, $p=0.02$); this result is in agreement with data obtained previously (Johns et al. 2001) where the time the vesicles spent near the PM was significantly lower than the time they spend further from the PM. The increase in the number of

visitors in turn affected the dwell time at the footprint of the cell which was significantly reduced by 26% in TeNt-LC overexpressing cells ($p=0.01$)

Then the vesicles were classified according to their mobility. The fraction of nearly immobile vesicles was reduced in TeNt expressing cells while the fraction of immobile-caged vesicles was increased (Fig. 33A). Although the changes were not significant, they were the opposite of the changes induced by PMA treatment or Munc13-1 overexpression.

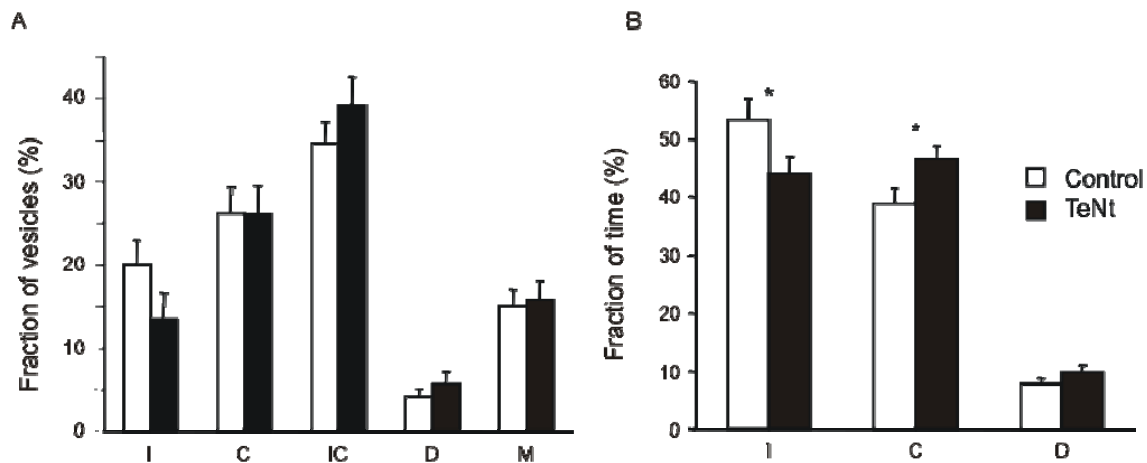


Fig. 33: TeNt-LC overexpression reduces the number of nearly immobile LDCVs. A, Fraction of vesicles in each type of motion. The fraction of nearly immobile vesicles was reduced but not significantly. B, Fraction of time spent in each type of motion; control, $N=25$, $n=553$; TeNt-LC, $N=22$, $n=453$. The fraction of time spent in the immobile state was significantly reduced and the fraction of time spent in the caged state was significantly increased. Error bars represent SEM; *, $p<0.05$.

The fraction of time the LDCVs spend in the immobile state was significantly reduced ($p=0.04$) in cells overexpressing TeNt-LC compared to control cells. On the other hand, LDCVs spend significantly more time in the caged state in TeNt-LC overexpressing cells ($p=0.04$) compared to control cells. These results are also the opposite to those obtained when cells were overexpressing Munc13-1 or treated with PMA (Fig. 33B).

These results support our hypothesis in which we state that nearly immobile vesicles represent primed vesicles and that caged vesicles represent docked but unprimed vesicles.

4. Discussion

In the present study, we asked the question whether primed vesicles had a different mobility than docked but unprimed vesicles. It has been previously shown that as they approach the PM, vesicles lose mobility and that immobilized vesicles are preferentially secreted. So, are primed vesicles immobile? To answer this question, we have devised a new method of analysis which allows us to monitor changes in mobility over time.

We have verified that the results acquired using TIRFM to measure secretion are qualitatively similar to those obtained using membrane capacitance recordings. This confirms the complementary role of TIRFM in measuring secretion, in addition to its irreplaceable role in monitoring presecretion events such as docking and priming.

4.1 The caging diameter: a novel method to analyze motion

We have devised a new method of analyzing the mobility of LDCVs in chromaffin cells which we call “caging diameter analysis”. The caging diameter is the maximal distance traveled by a vesicle in a sliding time window of six seconds. This method allowed us to obtain a CD for each position occupied by the vesicle over the time of observation. We were able to observe immediately changes in CD of vesicles in a cell towards a higher or lower CD (higher or lower mobility).

We were also able to distinguish between three different mobility states: Nearly immobile vesicles (I), caged vesicles (C) and vesicles with directed motion (D). In addition, we showed that, with this method, we could recognize two transitional states for vesicles: Immobile-caged vesicles (IC) and vesicles that have a mixture of the three main types of mobility states (M). The three main mobility states were recognized in previous studies (Burke et al. 1997; Steyer et al. 1999; Oheim et al. 2000; Johns et al. 2001). In these studies, the analysis of the LDCVs motion was made by calculating the MSD, which gave the diffusion coefficient and the caging radius of single vesicles or by the change in the fluorescence intensity for analyzing

the motion in the “z” direction. I have shown in the materials and methods section that analyzing the movement by calculating the MSD can yield incorrect results since the MSD calculation does not take into account the dynamic changes that could occur over time. This leads to false interpretations of the actual movement of the vesicle. In addition, one of the disadvantages of MSD analysis is that the accuracy of MSD values decrease with Δt due to averaging over smaller number of positions.

Oheim et al. (1999) succeeded in observing changes in mobility by plotting the 3-D diffusion coefficient over time, yet this method cannot differentiate between an immobile vesicle and one that has a directed motion for a relatively short period of time and having a low velocity.

More recently, Huet et al. (2006) have developed a method that seems to accurately describe the changes in mobility that vesicles undergo. This method depends on the calculation of three parameters: the diffusion coefficient to detect immobility, MSD curvature to detect caged motion and asymmetry to detect directed motion. Similar to our method of CD analysis, Huet et al. (2006) had to choose a time window of analysis, but this sliding window depended on the type of motion to be analyzed and thus was different for each case. Our sliding time window was in all cases six seconds long. This period of time was chosen after meticulous observation of the tracked vesicles. When we analyzed the CD with shorter time windows, it did not allow a reliable classification of the trajectory and the data were extremely noisy, whereas a larger time window did not allow the detection of brief specific motions due to averaging of the vesicle’s behavior. Also, Huet et al. (2006) had to verify and manually correct several of their sliding windows, while our method of analyzing the CD is fully automatic and human interference is minimal.

In the present work, I chose to ignore the motion in the “z” direction due to the error in determining the evanescent wave’s depth and because the fluorescence intensity was different from one vesicle to the other.

4.2 Secreted vesicles motion is different

By analyzing the CD of secreted and non secreted vesicles, I was able to show that secreted vesicles had a different mobility than that of non secreted ones.

Analyzing the size distribution of CDs, I found that there were four populations of CDs with different means and fractions of incidence. The first one with a mean of 56 nm represented the jitter inherent to our experimental system. The second population had a mean of 101 nm in both secreted and non secreted vesicles, but the incidence of this population was three times larger in secreted vesicles compared to non-secreted ones. This prompted us to think that this large population of CDs which is reduced in size when analyzing the mobility of non-secreted vesicles represented the mobility of primed vesicles (since the vesicles analyzed were exocytosed, they must have been primed prior to fusion). The third population had a mean of 220 nm and its incidence was four and a half times larger in non-secreted vesicles than in secreted ones. We thus assumed that this population of CDs represented the docked but not necessarily primed vesicles. The fourth population had a mean of 520 nm and its incidence was similar in secreted and non-secreted vesicles (less than 7%). This population represented the vesicles with large movements.

The CD corresponds to double the caging radius i.e. a CD of 101 nm would correspond to a caging radius of 50.5 nm. Our caging radii may differ slightly from those obtained by others (Oheim et al. 2000; Huet et al. 2006). This may be due the difference in the inherent jitter of the different experimental setups. The inherent jitter of our system was tested using beads fixed to the coverslip. The system jitter was tested (Oheim et al. 2000; Huet et al. 2006) and was found to be different from our calculated jitter value. This may be due to the difference in equipment, cameras, pixel size and signal to noise ratio. Oheim et al. (2000) uses a system that has a very low signal compared to ours and uses an image intensifier to correct for the low signal. This may affect the inherent jitter of the system and thereafter the values for caging radii obtained.

Our concern at this point was to verify whether the different molecular states corresponded to certain types of movements. To answer this question, we classified motion according to the size distribution of the CDs and we delimited each type of motion.

The first limit was set as the intersection point of the two populations of CDs which was 169 nm to differentiate nearly immobile vesicles (I) from caged ones (C). With the same reasoning we set 403 nm, the intersection point between the caged vesicles and those having a directed motion (D), as the CD that distinguishes these two populations.

Now that the method of analysis of the movement was established and that we found a notable difference in mobility between secreted thus primed vesicles and those that were not secreted, it remained to be proven that primed vesicles are indeed nearly immobile.

4.3 Priming leads to a reduction in the LDCV mobility

I enhanced priming using two independent methods: treatment with PMA and overexpression of Munc13-1. The cells used in both cases were recorded at rest. The cells were depolarized only at the end of the experiment to ascertain their viability and to monitor exocytosis. Also, I did not interfere with the $[Ca^{2+}]_i$ of the cells thus only enhanced priming affected the LDCVs mobility.

In PMA treated cells, there was a notable reduction in mobility after priming. This was seen as a reduction in the CD at 50% of PMA treated cells by 24% compared to control cells. To check which type of motion was affected, I classified the vesicles into the different mobility types (I, C, IC, D, M).

Docked vesicles are defined as those vesicles residing close to the PM (within 300 nm of the PM). These include both primed and unprimed vesicles. If our assumptions are correct and primed vesicles are nearly immobile while docked but unprimed ones are caged then the sum of immobile, caged, and immobile-caged vesicles represents the docked vesicles. After treatment with PMA this fraction of vesicles (I+C+IC) was unchanged compared to control which means that docking was not affected by PMA as observed previously (Gillis et al. 1996; Smith et al. 1997). In contrast, the fraction of immobile vesicles was increased by 19% compared to control whereas the fraction of caged and immobile caged vesicles was not markedly changed. This indicated that primed vesicles are indeed nearly immobile since PMA increases only the primed pool. If that is correct then the fraction of nearly immobile vesicles (primed vesicles) should be five times smaller than the fraction of caged vesicles (docked but unprimed vesicles, UPP) as shown previously by Ashery et al. 2000. Yet, I find that immobile

vesicles represented 45% of the total number of vesicles while caged vesicles represented only 8% in control condition. This would mean that the number of primed vesicles is 6 times larger than that of docked but unprimed vesicles (UPP). This discrepancy can be explained by the transfection method that I used to label the vesicles with NPY-mRFP. The transfection by means of the semliki virus system yields cells with a low density of stained vesicles ($0.1 \text{ vesicle}/\mu\text{m}^2$) which facilitates tracking. However, this method of transfection allows the staining of only the newly generated vesicles which were shown to be preferentially secreted thus primed (Duncan et al. 2003). Hence, it is likely that this method of transfection allows us to see a greater fraction of primed vesicles than docked ones. The fraction of vesicles with mixed behavior decreased by 45% compared to control, probably meaning that the probability that a vesicle transitions between different states decreases and that vesicles tend to remain longer in distinct molecular states (primed or docked). In agreement with the changes observed in the fractions of immobile and caged vesicles, the fraction of time spent in the immobile state was increased by 20% compared to control and the fraction of time spent in caged and directed motion was decreased after PMA treatment.

I then used a second independent method to enhance priming by overexpressing Munc13-1. Munc13-1 was found to increase the RRP size without affecting the UPP (Ashery et al. 2000). Overexpression of Munc13-1 caused a reduction in the CD by 28%, thus priming via Munc13-1 causes a reduction in the mobility of vesicles. As was the case with PMA treated cells, the number of immobile, caged and immobile-caged vesicles was unchanged in Munc13-1 overexpressing cells confirming previous findings that Munc13-1 does not affect docking. The fraction of immobile vesicles was increased by 68% in Munc13-1 overexpressing cells compared to control cells, while the fraction of caged vesicles was reduced by 48%. As Munc13-1 specifically promotes priming, then the increase in nearly immobile vesicles is due to the increase of the primed pool. Consistent with these results, the fraction of time spent in the nearly immobile state was increased by 33% and that spent in the caged state was decreased by 37%. The changes observed in Munc13-1 overexpressing cells were more marked than those observed in PMA treated cells. This could be because PMA is applied to the cell by perfusion and acts through second messengers while Munc13-1 is expressed in the cells and its action is direct. Thus, the effects observed in Munc13-1 overexpressing cells are larger compared to the

effects observed in PMA treated cells even though the analysis of the latter was done pair wise.

Taken together, the previous findings show that priming by PMA incubation or Munc13-1 overexpression increase the fraction of immobile vesicles while leaving the sum of the fractions of immobile, caged and immobile caged unchanged (Fig. 34). This strongly reinforces our hypothesis that primed vesicles are nearly immobile and that docked but unprimed ones are caged. This is also consistent with the results previously obtained (Steyer et al. 1997; Oheim et al. 1998; Johns et al. 2001) showing that immobilized vesicles were preferentially secreted. In these studies, the axial mobility (perpendicular to the PM) was analyzed rather than the lateral mobility (parallel to the PM). They found that as the vesicle approaches the PM its mobility diminished 4-fold. This suggests that a system or a matrix restricts the mobility of the vesicle at the PM. This matrix could either consist of the actin filaments or of the SNARE complex which is supposed to initiate priming. It has been shown that actin polymerization or depolymerization does not affect exocytosis from already immobilized vesicles (Oheim et al. 2000). More recently, it was shown that the actin skeleton provides a system to transport the vesicles from the cytoplasm to the subplasmalemmal areas and may play a role in bringing the vesicles to the docking sites (Giner et al. et al. 2005). But it has not been shown to play a role in the priming process. Therefore SNARE complex formation could be the second possible explanation for the immobilization of primed vesicles at the PM.

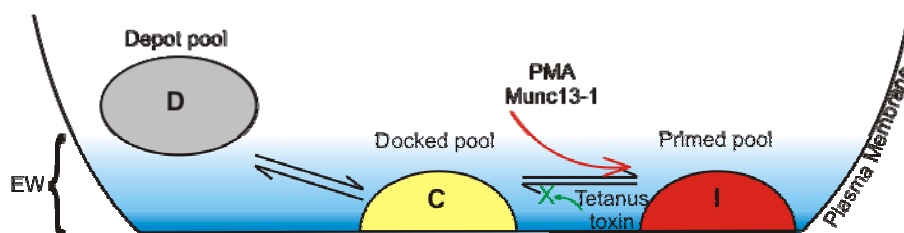


Fig. 34: The different molecular states have different mobilities. The primed pool is represented by the nearly immobile pool (I); the docked but unprimed pool (UPP) is represented by the caged pool (C); the depot pool is represented by the vesicles having a directed motion (D).

4.4 Mobility of LDCVs increases when priming is prevented

In order to confirm our hypothesis, I expressed the light chain of tetanus toxin in chromaffin cells. This toxin prevents synaptobrevin from interacting with syntaxin and SNAP-25 to form the SNARE complex. And since priming is thought to correspond to the SNARE complex formation, then preventing its formation should prevent priming. In this way, the fraction of nearly immobile vesicles should decrease and not increase. As expected, the CD at 50% of vesicles of cells expressing TeNt-LC was increased by 21.5% compared to control and although the increase was small it was significant. The fraction of nearly immobile vesicles was decreased by 30% in cells expressing TeNt-LC compared to control cells but this decreased was not significant. Yet the fraction of time spent in the nearly immobile state was significantly decreased by 15% and the fraction of time spent in the caged state was increased by 23%.

We expected that the changes in mobility would be large, but this was not the case. One reason could be that some vesicles were primed before tetanus toxin was expressed, and the formed SNARE complex did not allow the toxin to cleave synaptobrevin. We performed membrane capacitance recordings and found that cells expressing tetanus toxin showed no secretion, invalidating this. Another reason for the small changes in mobility could be that synaptotagmin, a vesicular protein, binds to the t-SNAREs in a constitutive manner before synaptobrevin does (Rickman et al. 2006). This forms a ternary SNARE complex (not including synaptobrevin) that tethers the vesicle to the PM and thus can mimic priming. This SNARE complex does not function as a fusogenic complex and is not Ca^{2+} dependent. It may rather be a preliminary process for the quick formation of the fusogenic SNARE complex. Thus the tethering function of synaptobrevin in the priming process could be replaced by that of synaptotagmin. However, although the changes were not spectacular, they were opposite to the changes observed when priming was enhanced. Again, this reinforced our hypothesis that primed vesicles correspond to nearly immobile vesicles. Our findings agree with those of Toonen et al. (2006) who found that expression of BoNt/C has a large effect on the axial mobility (perpendicular to the PM) of LDCVs whereas expression of TeNt-LC had a minor effect and the mobility of LDCVs was not increased.

I also found that there was a significant increase in the number of visitors (vesicles visible for less than 6 s) in TeNt-LC expressing cells compared to control cells. This was consistent with the increase in the fraction of time spent in directed motion and probably means that the equilibrium between the depot pool and the docked pool is disturbed in favor of the depot pool. So either docking is prevented or the undocking process is enhanced (Fig. 34). This finding agreed with that of Johns et al. (2001) where cleavage of synaptobrevin using tetanus toxin reduced the time the vesicles spend near the PM.

Finally, our method of analysis has shown that analyzing the lateral movement (parallel to the PM) is a good means to study priming since expressing tetanus toxin yielded visible changes in lateral mobility compared to the analysis of axial mobility where there was no visible effect of tetanus toxin (Toonen et al. 2006).

4.5 Perspectives

I have shown that the analysis of the caging diameter is a reliable tool to study the mobility of vesicles and that changes in mobility can be interpreted as changes in the molecular processes occurring prior to exocytosis. This can allow the investigation of numerous questions about docking and priming.

1- An important point that can be addressed is the calculation of the different rates of priming and docking. As mentioned in the introduction, the rate of priming was calculated using membrane capacitance recordings and the docking rate was obtained by simulation. Since we can distinguish clearly when a vesicle is in the primed pool or in the UPP, it should be possible -after optimization of the software- to calculate these rates in a more direct manner.

2- The analysis of the caging diameter can be a means to clarify the roles of proteins that showed conflicting effects such as complexin I and II. Genetic deletion of complexin I and II greatly decreased release efficiency (Reim et al. 2001).

In contrast, it has been found that overexpression of complexin in chromaffin cells led to a reduction in secretion (Archer et al. 2002). So it might be possible that complexin plays also a role in fusion pore opening.

3- In future studies, faster acquisition rates of recordings will be needed to be able to view subfractions of motion if they exist. This would help to elucidate the dilemma between studies stating that vesicles prior to exocytosis have a higher mobility (Allersma et al. 2006) where a recording frequency of 14 Hz was used whereas we and others (Steyer et al. 1999; Oheim et al. 2000; Johns et al. 2001) find that prior to exocytosis the vesicles are nearly immobile.

4- Besides its undisputed effect on fusion, calcium has also several effects on the processes occurring prior to fusion; TIRFM and analysis of the motion of LDCVs can elucidate these different effects by applying different concentrations of calcium through a patch pipette and observing the effect on motion. This approach could also be used to examine the role of ATP in presecretion events.

5- The role of Botulinum toxin B could also be studied since this toxin cleaves both synaptobrevin and synaptotagmin. This will probably prevent formation of any ternary SNARE complex whether fusogenic or not. What could be expected from such an experiment would be a great increase in the mobility of LDCVs and an absence of nearly immobile vesicles. The changes observed here should be greater than those observed when tetanus toxin was used.

6- Finally, it has recently been shown that using TIRFM, the observation of single molecules of proteins is possible (Mashanova et al. 2003; Xiao et al. 2006). Thus it could be possible to monitor these molecules from the place of their formation to the site of their interaction over time.

5. Summary

The fusion of vesicles with the presynaptic membrane represents the final event in the release of neurotransmitters and many other signalling molecules. Prior to fusion, synaptic vesicles undergo a series of maturation events leading to docking and priming.

Conventional electrophysiological studies have extensively studied the fusion step and provided important insights into the docking and priming processes. Up to now, no method has delivered direct information about the processes occurring prior to fusion. Total internal reflection fluorescence microscopy allows the real-time visualization of fluorescent particles with a very high signal to noise ratio. The use of TIRFM to observe the behaviour of fluorescently marked vesicles allows us to study the processes occurring prior to fusion with greatly enhanced fidelity.

In the present study, we visualize fluorescent large dense-core vesicles in bovine chromaffin cells using TIRFM to observe their movements over time. We analyze the motion of LDCVs using a novel technique we called the “caging diameter” analysis that permits us to observe the dynamic changes in mobility occurring over time. Using this method, we have been able to recognize vesicles with different types motion: a) nearly immobile vesicles, b) caged vesicles, c) immobile-caged vesicles, d) vesicles with directed motion and e) vesicles with mixed types of motion.

It has previously been shown in chromaffin cells that as the vesicles approach the plasma membrane, they tend to immobilize and that immobilized vesicles preferentially fuse with the plasma membrane. It has also been proposed that priming is the step in which the SNARE complex is formed and that this complex tightly tethers the vesicles to the plasma membrane. This suggested that priming should lead to immobilization of vesicles. We have tentatively assigned the behaviour we termed “nearly immobile” to primed vesicles and the “caged” behaviour to the docked but unprimed state. To verify this hypothesis, we used a pharmacological approach to enhance priming. We treated cells with either a phorbol ester or we have overexpressed Munc13-1 in bovine chromaffin cells; these two methods are known to enhance priming by increasing the size of the primed pool without affecting the

docked but unprimed pool. Using these treatments, we found that the percentage of nearly immobile vesicles was increased. As PMA and Munc13-1 increase only the primed pool and as only the fraction of nearly immobile vesicles was increased, we conclude that primed vesicles are nearly immobile. With similar reasoning, we conclude that docked but unprimed vesicles are indeed caged vesicles and that vesicles with directed motion are neither primed nor docked and thus belong to the depot pool.

To challenge our hypothesis, we have prevented priming by expressing the light chain of tetanus toxin in bovine chromaffin cells. This toxin cleaves synaptobrevin and prevents it from participating in the SNARE complex formation. We found that the mobility of LDCVs was increased. The fraction of nearly immobile vesicles was decreased as well as the fraction of time spent in the immobile state. The fraction of time spent in the caged state was increased. Although the changes were not spectacular, they were the opposite from the changes observed when priming was enhanced. This confirms our hypothesis that priming corresponds to immobilization of vesicles and agrees well with the previous findings that immobilized vesicles preferentially fuse with the plasma membrane.

6. Literature

Allersma, M., Bittner, MA, Axelrod, D and Holz, RW (2006). "Motion Matters: Secretory Granule Motion Adjacent to the Plasma Membrane and Exocytosis." Mol Biol Cell **17**: 2424–2438.

Almers, W. (2001). "Fusion needs more than SNAREs." Nature **409**(6820): 567-8.

Aravamudan, B., Fergestad, T., Davis, W.S., Rodesch, C.K., and Broadie, K. (1999). "Drosophila UNC-13 is essential for synaptic transmission." Nat Neurosci **2**: 965-971.

Archer, D. A., Graham, M.E., and Burgoyne, R.D. (2002). "Complexin regulates the closure of the fusion pore during regulated vesicle exocytosis." J Biol Chem **277**: 18249-18252.

Artalejo, C. R., Elhamdani, A., and Palfrey, H. C. (2002). "Sustained stimulation shifts the mechanism of endocytosis from dynamin-1-dependent rapid endocytosis to clathrin- and dynamin-2-mediated slow endocytosis in chromaffin cells." PNAS **99**(9): 6358–6363.

Ashery, U., Betz, A, Xu, T, Brose, N, and Rettig, J. (1999). "An efficient method for infection of adrenal chromaffin cells using the Semliki Forest virus gene expression system." Eur J Cell Biol **78**: 525-532.

Ashery, U., Varoqueaux, F, Voets, T, Betz, A, Thakur, P, Koch, H, Neher, E, Brose, N, and Rettig, J (2000). "Munc13-1 acts as a priming factor for large dense-core vesicles in bovine chromaffin cells." EMBO J **19**: 3586-3596.

Augustin, I., C. Rosenmund, T. C. Sudhof and N. Brose (). (1999). "Munc13-1 is essential for fusion competence of glutamatergic synaptic vesicles." Nature **400**(6743): 457-61.

Axelrod, D. (2001). "Total internal reflection fluorescence microscopy in cell biology." Traffic **2**(11): 764-74.

Bennett, M. K., and Scheller, R. H. (1993). "The molecular machinery for secretion is conserved from yeast to neurons." Proc. Natl. Acad. Sci. **90**: 2559-2563.

Betz, A., Ashery, U., Rickmann, M., Augustin, I., Neher, E., Sudhof, T.C., Rettig, J., and Brose, N. (1998). "Munc13-1 is a presynaptic phorbol ester receptor that enhances neurotransmitter release." Neuron **21**: 123-136.

Beutner, D. a. T. M. (2001). "The presynaptic function of mouse cochlear inner hair cells during development of hearing." J Neurosci **21**(13): 4593-9.

Borst, J. G., F. Helmchen and B. Sakmann (1995). "Pre- and postsynaptic whole-cell recordings in the medial nucleus of the trapezoid body of the rat." J Physiol **489**((Pt 3)): 825-40.

Breidenbach, M. A., and Brunger, A.T. (2005). "New insights into clostridial neurotoxin–SNARE interactions." TRENDS in Molecular Medicine **11**(8): 377-381.

Brose, N., C. Rosenmund and J. Rettig (2000). "Regulation of transmitter release by Unc-13 and its homologues." Curr Opin Neurobiol **10**(3): 303-11.

Burke, N., Han, W, Li, D, Takimoto, K, Watkins, SC, and Levitan, ES. (1997). "Neuronal peptide release is limited by secretory granule mobility." Neuron **19**: 1095-1102.

Cahill, A. L., Eertmoed, A. L., Mangoura, D., and Perlman, R. L. (1996). "Differential regulation of phenylethanolamine N-methyltransferase expression in two distinct subpopulations of bovine chromaffin cells." J Neurochem **67**(3): 1217-24.

Calakos, N., Schoch, S., Sudhof, T.C., and Malenka, R.C. (2004). "Multiple roles for the active zone protein RIM1alpha in late stages of neurotransmitter release." Neuron **42**: 889-896.

Cole, T. J., . Blendy, J. A, Monaghan, A. P., Krieglstein, K., Schmid, W., Aguzzi, A., Fantuzzi, G., Hummler, E., Unsicker, K., and Schutz, G. (1995). "Targeted disruption of the glucocorticoid receptor gene blocks adrenergic chromaffin cell development and severely retards lung maturation." Genes Dev **9**(13): 1608-21.

De Potter, W. P., Partoens, P., Schoups A., Llona I., and Coen E.P. (1997). "Noradrenergic neurons release both noradrenaline and neuropeptides from a single pool: the large dense cored vesicles." Synapse **24**: 44-55.

Dulubova, I., Sugita, S., Hill, S., Hosaka, M., Fernandez, I., Südhof, T.C., and Rizo, J. (1999). "A conformational switch in syntaxin during exocytosis: role of Munc18." EMBO J **18**: 4372-4382.

Duncan, R., Greaves, J, Wiegand, UK, Matskevich, I, Bodammer, G, Apps, DK, Shipston, MJ, and Chow, RH (2003). "Functional and spatial segregation of secretory vesicle pools according to vesicle age." Nature **422**: 176-180.

Garner, C. C., Kindler, S., and Gundelfinger, E. D. (2000). "Molecular determinants of presynaptic active zones." Curr Opin Neurobiol **10**(3): 321-327.

Gillis, K., Mossner, R, and Neher, E. (1996). "Protein kinase C enhances exocytosis from chromaffin cells by increasing the size of the readily releasable pool of secretory granules." Neuron **16**: 1209-1220.

Giner, D., Neco, P., Francés, M.M., López, I., and Viniegra S. and a. L. M. Gutiérrez (2005). "Real-time dynamics of the F-actin cytoskeleton during secretion from chromaffin cells." Journal of Cell Science **118**: 2871-2880.

Hanson, P. I., Heuser, J.E., and Jahn, R. (1997). "Neurotransmitter release: four years of SNARE complexes." Curr Opin Neurobiol **7**: 310-315.

Hay, J., and Scheller, RH. (1998). "SNAREs and NSF in targeted membrane fusion." Curr Opin Cell Biol **9**: 505-512.

Heidelberger, R., Heinemann, C., Neher, E., and Matthews, G. (1994). "Calcium dependence of the rate of exocytosis in a synaptic terminal." Nature **371**(6497): 513-5.

Huet, S., Karatekin, E, Tran, VS, Fanget, I, Cribier, S, and Henry, JP (2006). "Analysis of transient behavior in complex trajectories: application to secretory vesicle dynamics." Biophys J(Epub ahead of print).

Jahn, R., Lang, T., and Sudhof, T. C. (2003). "Membrane fusion." Cell **112**(4): 519-33.

Johns, L., Levitan, ES, Shelden, EA, Holz, RW, and Axelrod, D (2001). "Restriction of secretory granule motion near the plasma membrane of chromaffin cells." J Cell Biol **153**: 177-190.

Junge, H. J., Rhee, J.S., Jahn, O., Varoqueaux, F., Spiess, J., Waxham, M.N., Rosenmund, C., and Brose, N. (2004). "Calmodulin and Munc13 form a Ca²⁺ sensor/effector complex that controls short-term synaptic plasticity." Cell **118**: 389-401.

Kits, K. S., and Mansvelder, H. D. (2000). "Regulation of exocytosis in neuroendocrine cells: spatial organization of channels and vesicles, stimulus-secretion coupling, calcium buffers and modulation." Brain Res Brain Res Rev **33**(1): 78-94.

Lonart, G., and Sudhof, T. C. (2000). "Assembly of SNARE core complexes prior to neurotransmitter release sets the readily releasable pool of synaptic vesicles." J. Biol. Chem. **275**: 27703-27707.

Low, P., Norlin, T. , Risinger, C., Larhammar, D., Pieribone, V. A., Shupliakov, O., and Brodin, L. (1999). "Inhibition of neurotransmitter release in the lamprey reticulospinal synapse by antibody-mediated disruption of SNAP-25 function." Eur J Cell Biol **78**(11): 787-93.

Madison, J. M., Nurrish, S., and Kaplan, J.M. (2005). "Unc-13 interaction with syntaxin is required for synaptic transmission." Curr Biol **15**: 2236-2242.

Martelli, A. M., Baldini, G., Tabellini, G., Koticha, D., Bareggi, R., and Baldini, G. (2000). "Rab3A and Rab3D control the total granule number and the fraction of granules docked at the plasma membrane in PC12 cells." Traffic **1**: 976-986.

Mashanova, G. I., Taconb, D., Knighta, A. E., Peckhamb, M., and Molloy, J. E. (2003). "Visualizing single molecules inside living cells using total internal reflection fluorescence microscopy." Methods **29**(2): 142-152.

Nagai, T., Ibata, K., Park, E. S. , Kubota, M., Mikoshiba, K., and Miyawaki, A. (). (2002). "A variant of yellow fluorescent protein with fast and efficient maturation for cell-biological applications." Nat Biotechnol **20**(1): 87-90.

Nagy, G., Matti, U., Nehring, R.B., Binz, T., Rettig, J., Neher, E., and Sorensen, J.B. : (2002). "Protein kinase C-dependent phosphorylation of synaptosome-associated protein of 25 kDa at Ser187 potentiates vesicle recruitment." J Neurosci **22**: 9278-9286.

Nagy, G., Reim, K., Matti, U., Brose, N., Binz, T., Rettig, J., Neher, E., and Sorensen, J.B. (2004). " Regulation of releasable vesicle pool sizes by protein kinase A-dependent phosphorylation of SNAP-25." Neuron **41**: 417-429.

Oberhauser, A. F., Monck, J. R., and Fernandez, J. M. (1992). "Events leading to the opening and closing of the exocytotic fusion pore have markedly different temperature dependencies. Kinetic analysis of single fusion events in patch-clamped mouse mast cells." Biophys J **61**(3): 800-9.

Oheim, M. (2001). "Imaging transmitter release. I. Peeking at the steps preceding membrane fusion." Lasers Med Sci **16**(3): 149-158.

Oheim, M., and Stuhmer, W (2000). "Tracking chromaffin granules on their way through the actin cortex." Eur Biophys J **29**: 67-89.

Oheim, M., Loerke, D, Stuhmer, W, and Chow, RH. (1998). "The last few milliseconds in the life of a secretory granule. Docking, dynamics and fusion visualized by total internal reflection fluorescence microscopy (TIRFM)." Eur Biophys J **27**: 83-98.

Oheim, M., Loerke, D., Stühmer, W., and Chow, R. H. (1999). "Multiple stimulation-dependent processes regulate the size of the releasable pool of vesicles." Eur Biophys J **28**: 91-101.

Qian, H., Sheetz, MP., and Elson, EL. (1991). "Single particle tracking. Analysis of diffusion and flow in two-dimensional systems." Biophys J **60**: 910-921.

Reim, K., Mansour, M., Varoqueaux, F., McMahon, H.T., Südhof, T.C., Brose, N., and Rosenmund (2001). "Complexins Regulate a Late Step in Ca²⁺-Dependent Neurotransmitter Release." Cell **104**: 71-81.

Rettig, J., and Neher, E (2002). "Emerging roles of presynaptic proteins in Ca⁺⁺-triggered exocytosis." Science **298**: 781-785.

Rhee, J. S., Betz, A., Pyott, S., Reim, K., Varoqueaux, F., Augustin, I., Hesse, D., Südhof, T.C., Takahashi, M., Rosenmund, C., and Brose, N. (2002). "Beta phorbol ester- and diacylglycerol-induced augmentation of transmitter release is mediated by Munc13s and not by PKCs." Cell **108**: 121-133.

Richmond, J. E., Davis, W.S., and Jorgensen, E.M. (1999). "Unc-13 is required for synaptic vesicle fusion in *C. elegans*." Nat Neurosci **2**: 959-964.

Rickman, C., Jimenez, J.L., Graham, M., E. , Archer, D.A., Soloviev, M., Burgoyne, R.D., and Davletov, B. (2006). "Conserved Prefusion Protein Assembly in Regulated Exocytosis." Mol Biol Cell **17**: 283–294.

Schiavo, G., Matteoli, M, and Montecucco, C (2000). "Neurotoxins Affecting Neuroexocytosis." PHYSIOLOGICAL REVIEWS **80**(2): 717-766.

Schluter, O. M., Basu, J., Sudhof, T.C., and Rosenmund, C. (2006). "Rab3 superprimes synaptic vesicles for release: implications for short-term synaptic plasticity." J Neurosci **26**: 1239-1246.

Schluter, O. M., Schmitz, F., Jahn, R., Rosenmund, C., and Sudhof, T.C. (2004). "A complete genetic analysis of neuronal Rab3 function." J Neurosci **24**: 6629-6637.

Schoch, S., Castillo, P.E., Jo, T., Mukherjee, K., Geppert, M., Wang, Y., Schmitz, F., Malenka, R.C., and Sudhof, T.C. (2002). "RIM1alpha forms a protein scaffold for regulating neurotransmitter release at the active zone." Nature **415**: 321-326.

Schutz, D., Zilly, F., Lang, T., Jahn, R., and Bruns, D. (2005). "A dual function for Munc-18 in exocytosis of PC12 cells." Eur J Neurosci **21**: 2419-2432.

Siegelbaum, S. A., and Kandel, E. R. (1991). "Learning-related synaptic plasticity: LTP and LTD." Curr Opin Neurobiol **1**(1): 113-20.

Smith, C., and Neher, E. (1997). "Multiple forms of endocytosis in bovine adrenal chromaffin cells." J Cell Biol **139**(4): 885-94.

Smith, C., Moser, T, Xu, T, and Neher, E. (1998). "Cytosolic Ca²⁺ acts by two separate pathways to modulate the supply of release-competent vesicles in chromaffin cells." Neuron **20**: 1243-1253.

Sollner, T., Whiteheart, S. W., Brunner, M., Erdjument-Bromage, H., Geromanos, S., and P. Tempst, and Rothman, J. E. (1993). "SNAP receptors implicated in vesicle targeting and fusion." Nature **362**: 318-324.

Speidel, D., Bruederle, C.E., Enk, C., Voets, T., Varoqueaux, F., Reim, K., Becherer, U., Fornai, F., Ruggieri, S., Holighaus, Y., Weihe, E., Bruns, D., Brose, N., and Rettig, J. (2005). "CAPS1 regulates catecholamine loading of large dense-core vesicles." Neuron **46**: 75-88.

Stevens, D. R., Wu, Z.X., Matti, U., Junge, H.J., Schirra, C., Becherer, U., Wojcik, S.M., Brose, N., and Rettig, J. (2005). "Identification of the minimal protein domain required for priming activity of Munc13-1." Curr Biol **15**: 2243-2248.

Steyer, J., and Almers, W (1999). "Tracking single secretory granules in live chromaffin cells by evanescent-field fluorescence microscopy." Biophys J **76**: 2262-2271.

Steyer, J. A., Horstmann, H., and ALMERS, W. (1997). "Transport, docking and exocytosis of single secretory granules in live chromaffin cells." Nature **388**: 474-478.

Sutton, R. B., Fasshauer, D., Jahn, R., and Brunger, A. T. (1998). "Crystal structure of a SNARE complex involved in synaptic exocytosis at 2.4 Å resolution." Nature **395**: 347-353.

Tadokoro, S., Nakanishi, M., and Hirashima, N. (2005). "Complexin II facilitates exocytotic release in mast cells by enhancing Ca²⁺ sensitivity of the fusion process." J Cell Sci **118**: 2239-2246.

Toomre, D., and Manstein, D. J. (2001). "Lighting up the cell surface with evanescent wave microscopy." Trends Cell Biol **11**(7): 298-303.

Toonen, R., de Vries, KJ, Zalm, R, Südhof, TC, and Verhage, M (2005). "Munc18-1 stabilizes syntaxin 1, but is not essential for syntaxin 1 targeting and SNARE complex formation. ." J Neurochem **93**: 1393-1400.

Toonen, R., Kochubey, O, de Wit, H, Gulyas-Kovacs, A, Konijnenburg, B, Sorensen, JB, Klingauf, J, and Verhage, M (2006). "Dissecting docking and tethering of secretory vesicles at the target membrane." EMBO J **25**: 3725-3737.

Voets, T. (2000). "Dissection of three Ca²⁺-dependent steps leading to secretion in chromaffin cells from mouse adrenal slices." Neuron **28**(2): 537-45.

Voets, T., Toonen, RF, Brian, EC, de Wit, H, Moser, T, Rettig, J, Südhof, TC, Neher, E, and Verhage, M (2001). "Munc18-1 promotes large dense-core vesicle docking." Neuron **31**: 581-591.

Washbourne, P., Cansono, V, Graham, ME, Burgoyne, RD, and Wilson, MC. (2001). "The cysteines of SNAP-25 are required for SNARE complex disassembly and exocytosis, not for membrane targeting." Biochem J **357**: 625–634.

Xiao, M., Phong, A., Ha, C., Chan, T., Cai, D., Leung, L., Wan, E., Kistler, A.L., DeRisi, J.L., Selvin, P.R., and Kwok, P. (2006). "Rapid DNA mapping by fluorescent single molecule detection." Nucleic Acids Research **0**(0): 1-12.

Xu, T., Rammner, B., Margittai, M., Artalejo, A. R., Neher, E., and Jahn, R. (1999). "Inhibition of SNARE complex assembly differentially affects kinetic components of exocytosis." Cell **99**(7): 713-22.

Zenisek, D., Steyer, JA, and Almers, W (2000). "Transport, capture and exocytosis of single synaptic vesicles at active zones." Nature **406**: 849-854.

Curriculum Vitae

Personal data:

Name: Shahira Nofal Ibrahim El Sayed
Date of birth: 1-12-1974
Place of birth: Burundi
Adress: Gerhart-Hauptmann str. 24, 67663 Kaiserslautern
Marital status: married
Nationality: Egyptian

Education:

2003 Master of science in Pharmacology from the Faculty of Pharmacy, University of Cairo, Egypt
2000 Premaster degree in Pharmacology from Faculty of Pharmacy, University of Cairo, Egypt
1997 Bachelor of Science in Pharmaceutical sciences (very good) from the Faculty of Pharmacy, University of Cairo, Egypt
1992 Baccaalaureat degree, scientific section (good) from the Lycee Francais Saint-Louis in Stockholm, Sweden

Research work:

December 1997-April 2003 Research assistant in the Department of Acute Toxicology in the National Organization of Drug Control And Research, Cairo, Egypt
December 2003-present Research work for the PhD in the Department of Prof. Dr. Jens Rettig in the institute of Physiology Geb. 59 the University of Saarland, Homburg, Germany

Publications

Shahira Nofal*, Ute Becherer*, Detlef Hof, Ulf Matti and Jens Rettig

Primed vesicles can be distinguished from docked vesicles by analyzing their mobility.

Journal of Neuroscience, article accepted.

*=equal contribution

Shahira Nofal, Ute Becherer, Detlef Hof, Ulf Matti and Jens Rettig

Real-time visualization of priming reaction of large dense-core vesicles

5th Forum of European Neuroscience, Vienna, Austria, 2006.